ELSEVIER

Contents lists available at ScienceDirect

Atmospheric Research

journal homepage: www.elsevier.com/locate/atmosres





Luminosity with large amplitude pulses after the initial breakdown stage in intracloud lightning flashes

Maribeth Stolzenburg*, Thomas C. Marshall, Sampath Bandara, Raymond Siedlecki

Department of Physics & Astronomy, University of Mississippi, University, MS, USA

ARTICLE INFO

Keywords: Intracloud lightning WWLLN Lightning luminosity Terrestrial gamma-ray flash

ABSTRACT

Optical data are presented for two intracloud flashes in which there were five events having large amplitude, bipolar electric field change (E-change) pulses and strong VHF emissions. These bright events occurred 18.98-67.33 ms after the initiating event and 10-59 ms after the end of the initial breakdown stage. The three largest events were coincident with WorldWide Lightning Location Network detections of the sort previously associated with terrestrial gamma-ray flashes (TGFs); these pulses had range-normalized E-change amplitudes of 8.73, 8.33, and 3.81 V/m and estimated peak current magnitudes of 262, 250, and 114 kA. The other two events were 3.20 and 1.62 V/m (96 and 49 kA). All five events have bright enhanced luminosity (>10% above background) for durations of 0.7-1.20 ms, similar to durations of their moderate-to-strong VHF emissions. Full-frame peak intensities are factors of 1.82-4.46 times the background level. Maximum cumulative intensity in the camera frame occurs 84–98 μ s after the *E*-change peak in three cases and ranges from $-10~\mu$ s (before) to $+115~\mu$ s (after) for all cases. Notably, in all five events the luminosity starts increasing when the E-change and VHF sensors begin detecting oscillations, 135-550 µs before the E-change peak. Pulse locations of each event extend through 3.6 to 4.3 km depth, starting below and ending above the altitude of flash initiation, and the linear pathlength of activity with these events is estimated at 8.9-11.3 km within radar reflectivities of 20-40 dBZ. Although these events are not initial breakdown pulses, their luminosity could be visible from satellite-borne instruments and they may be associated with TGFs.

1. Introduction

Fishman et al. (1994) discovered terrestrial gamma-ray flashes (TGFs) and showed they were probably connected to thunderstorms. TGFs are short bursts (< 1 ms) of gamma-ray photons that originate in the Earth system (Fishman et al., 2011). Using electric field change (Echange) data, Stanley et al. (2006) found that many TGFs are associated with typical intracloud (IC) lightning discharges that move negative charge upward from the cloud's negative charge region to an upper positive charge region. Lu et al. (2010) documented a case of a TGF occurring within 5 ms of the IC flash initiation "during the early stage of an upward propagating negative leader." More recently, Cummer et al. (2015) used magnetic field change (B-change) measurements to show that three TGFs "were produced several milliseconds" after flash initiation, "when the leaders reached 1-2 km in length"; the TGFs occurred at altitudes of 9-11 km. In keeping with previous terminology, herein we refer to the E-change pulses produced by the initial leader as initial breakdown pulses (IB pulses or IBPs), and to the time period of the IBPs as the IB stage of the flash (e.g., Marshall et al., 2013).

Marshall et al. (2013) studied 10 IC flashes (deemed likely candidates for producing TGFs) and found IB pulses occurred in the first 2-7 ms after flash initiation and spanned depths of 1260-4270 m, with flash initiation altitudes of 7.0–10.9 km and upper IBP altitudes of 10.2–14.7 km. Marshall et al. (2013) concluded that the "the IB stage in IC flashes can be defined by the time needed for the initial leader to span the gap between the main negative and upper positive cloud charges." More precisely, in typical IC flashes the initiation altitude is at a local maximum in the vertical electric field magnitude near the top of a negative charge region, while the upper extent of the IBPs is near the altitude of the electric potential well in an upper positive charge region (e.g., Coleman et al., 2003). Once the initial leader reaches the altitude of the potential well, the IB stage ends and a negative stepped leader extends mostly horizontally in the well, through the upper positive charge region. Other examples of IC flashes showing the initial leader reaching the upper potential well (and hence the end of the IB stage) are found in Stolzenburg et al. (2016); the IB stages of their two flashes had

E-mail address: mstolzen@olemiss.edu (M. Stolzenburg).

https://doi.org/10.1016/j.atmosres.2021.105982

^{*} Corresponding author.

durations of about 5 ms. Shi et al. (2019, 2020) also have examples of this vertical progression through the first few ms during IB stages in IC flashes. On the basis of these and other studies, the IB stage durations of IC flashes are typically <10 ms and most of the large amplitude pulses in IC flashes are IBPs.

Large amplitude E-change pulses can also occur more than 10 ms after IC flash initiation and after the IB stage has ended, as shown in Marshall et al. (2013), Shao and Krehbiel (1996), and many prior works. These later large pulses likely develop differently from IBPs, as described in Shao and Krehbiel (1996), although some details are still unknown. Villanueva et al. (1994) used wideband E-change measurements to investigate the full evolution of E-change pulses in IC flashes; their work was the culmination of similar, prior studies by Kitagawa and Brook (1960) and Bils et al. (1988). Villanueva et al. (1994) studied 17 IC flashes in New Mexico and Florida and defined three categories of Echange pulses, Large (E_L), Medium (E_M), and Small (E_S), based on peakto-peak amplitude. For each flash the average peak-to-peak amplitude, E₅, of the five largest pulses was determined. Then "Large" pulses had E_L $\geq 0.5E_5$, "Medium" pulses had $0.25E_5 \leq E_M < 0.5E_5$, and "Small" pulses had $E_S < 0.25E_5$. Based in part on the prior studies, Villanueva et al. (1994) also divided each flash into "early" stage (first 80 ms) and "late" stage (the rest of the flash). (These same two stages are sometimes referred to as "active" and "final.") It was found that there were, on average, about 10 Large pulses in each IC flash and that 80-100% of these occurred in the early stage of most flashes. Notably, Villanueva et al. (1994) stated that 53% and 45% of Large IC pulses occurred in the first 5 ms of New Mexico and Florida flashes, respectively, which suggests those pulses were IBPs (and also supports the final statement in the previous paragraph). Other Large IC pulses in the early stage were apparently a form of early "K"-events, as studied by Shao and Krehbiel (1996), which repeatedly move negative charge vertically upward and sometimes have appreciable electric field changes (e.g., events D, G, H in Flash A of Shao and Krehbiel, 1996)). In the late stage of IC flashes, Villanueva et al. (1994) saw many small (or "kleine") pulses, called Kchange pulses (following Kitagawa and Brook (1960); see Akita et al. (2010) for a review). On the basis of their statistical analyses Villanueva et al. (1994) noted that Large pulses "tended to avoid" the late stage, which "indicates" that the Large IC pulses "are not produced by K processes" (the processes that result in K-change pulses). Using a VHF broadband interferometer and VHF lightning mapping array, Stock et al. (2014) fully mapped and described many 'K-events' during the late stage of one IC flash; all 39 of their K-events with VHF duration >200 us occurred more than 130 ms after flash initiation. (No E-change data were available for the Stock et al. (2014) flash, so it is not known whether there was a sizable field change pulse accompanying their events.) Akita et al. (2010) also documented and mapped several Kchange events, all of which occurred more than 140 ms after the flash beginning and were accompanied by relatively small field changes.

To our knowledge, there have been only a few detected TGFs (thus far in the literature) that could be given an occurrence and/or location context in the B-change or E-change data of the developing lightning flash, specifically, those mentioned above examined by Lu et al. (2010) and Cummer et al. (2015), and the recent work by Østgaard et al. (2021). All these TGFs occurred within the first 2-4 ms of the IB stage of the IC flash, were 1-2 km above the flash initiation altitude, and were approximately time coincident with an IBP. It is not yet known whether all satellite-detected TGFs occur during the IB stage of an IC flash. The lack of information about when and where TGFs occur during a flash is largely due to the difficulty in having both a satellite to measure gamma emissions and sensors to measure E-change or B-change data of the entire flash duration. To help solve this problem, Lyu et al. (2016) proposed a proxy for the TGF, namely a pulse in E-change or B-change data with a waveform fitting the characteristics of a positive Energetic In-cloud Pulse (+EIP). +EIPs were first defined by Lyu et al. (2015) as a class of radio pulses occurring in IC flashes having five properties: bipolar waveform, high estimated peak current (>200 kA), duration of $40{\text -}100~\mu s$ (mean of 55 μs), correct ratio of initial peak to main peak, and correct "isolation ratio" (see Lyu et al. (2015) for details). Lyu et al. (2015) determined that the altitudes of 27 + EIPs ranged from 9.2 km to 13.3 km, with a mean of 11.4 km. This range is in reasonable agreement with the altitude range (7.0–14.7 km) of IBPs in IC flashes studied by Marshall et al. (2013) and the average altitude (9.1 km) of the largest IBP in 32 IC flashes studied by Smith et al. (2018). Lyu et al. (2016) presented evidence supporting the hypothesis that +EIPs are the radio signal of a TGF event: three TGFs were coincident in time and location with +EIPs. Lyu et al. (2016) also found 12 + EIPs that occurred during the IB stage of IC flashes, and Tilles et al. (2020) have documented another example with multiple types of data. Thus, using +EIPs as a proxy for a TGF event offers an excellent way of expanding our understanding of possible TGF occurrence and location contexts within IC flashes.

Earlier work by Connaughton et al. (2013) also determined other possible proxy data for TGF occurrences. Connaughton et al. (2013) found coincidences between TGFs detected by the Fermi spacecraft (Fishman et al., 2011) and events detected by the World Wide Lightning Location Network (WWLLN). WWLLN measures the time and location of "lightning strokes" to "within a few kilometers and tens of microseconds" using VLF E-change measurements (Hutchins et al., 2012). In particular, Connaughton et al. (2013) found that the shortest TGFs (with durations <150 μ s) had an associated WWLLN event "over 50% of the time" and had estimated event currents >150 kA (based on Abarca et al., 2010). Unfortunately, there was no information about the lightning occurrence context (timing or location) for the TGFs studied by Connaughton et al. (2013) or the flash type (cloud-to-ground or IC). A study of IC flashes in which WWLLN-detected events occur should improve our understanding of TGFs.

While IC flashes are relatively common, time-correlated electromagnetic and optical observations are rare in the literature and are focused primarily on the IB stage. Using E-change sensors and a high speed video camera operating at 50,000 frames/s, Stolzenburg et al. (2013a) found that there was a burst of light coincident with largeamplitude IBPs in three IC flashes (and twelve cloud-to-ground flashes). Using the same instrumentation, Stolzenburg et al. (2016) studied the IC IBPs of four hybrid flashes; the IBPs were selected because their large E-change amplitudes and large charge moment changes suggested they might be associated with TGFs. Wilkes et al. (2016) used an E-change sensor and a wide-aperture avalanche photodiode (10 ns response time) to study cumulative intensity "of the cloud surface" due to IBPs in eight IC flashes (and seven ground flashes). Using E-change sensors and a video camera operating at 150,000 frames/s, Stolzenburg et al. (2021) studied the cumulative intensity of the first 10-50 ms of five IC flashes, focusing mainly on initiation events and IBPs. These four studies found that the luminosity pulse of IBPs had durations ranging between 200 and 1700 µs, which are at least 5-10 times longer than the duration of the E-change pulse of the corresponding IBP. Also, the peak of the luminosity trailed the E-change peak by 80-270 µs. Together, these findings indicate that an IBP starts a current that causes the detectable luminosity.

Data and analyses from the Atmosphere-Space Interactions Monitor (ASIM), onboard the International Space Station orbiting Earth at about 400 km altitude, have provided new details of lightning luminosity associated with TGFs. ASIM has two main sensors: the modular X- and gamma-ray sensor to measure TGF photons and the modular multispectral imaging array that measures photons in three wavelength ranges: 180–235 nm, 337 \pm 2.5 nm, and 777 \pm 1.5 nm (Neubert et al., 2020). Neubert et al. (2020) and Østgaard et al. (2019) have examined ASIM data for a TGF and Elve that were both caused by a high-current, high luminosity lightning event (as indicated by a large optical pulse in the 777 nm channel). One of the main results of both these studies is that "the current pulse that generates the optical pulse has its onset simultaneous with the TGF (within the relative timing uncertainty)" (of \pm 80 μ s), "but develops and reaches its peak intensity after the TGF"

(Østgaard et al., 2019). Østgaard et al. (2021) extended their prior study to show that the TGF associated with the Elve "was produced just before or most likely simultaneously with" a + EIP. Based on the detection of three relatively small pulses in B-change data that were coincident with the first light detected in the 777 nm channel, Østgaard et al. (2021) determined that the TGF started 1 ms after the beginning of the IC flash.

In this work, we investigate high-speed video and multi-station electromagnetic data for five very large amplitude E-change pulses in two IC flashes. Each of the five E-change pulses occurred near the beginning of bright luminosity bursts; enhanced luminosity greater than 10% above background and strong VHF emissions have durations exceeding 700 μ s, much longer than the accompanying large E-change pulse with duration of $\sim\!200~\mu s$. Only one other event in each of these two flashes had detected luminosity exceeding 50% above background. Unlike prior optical studies of IC flashes, these five bright events and large pulses occurred well after the IB stage of each flash but within the first 80 ms after flash initiation. Located pulses of these events show they travelled through substantial depths of approximately 4 km and horizontal extents averaging about 10 km. No space-borne gamma-ray detection data were available for these events. However, three of the five pulses had coincident WWLLN detections, and at least two of the pulses fit criteria of +EIPs according to Lyu et al. (2015, 2016). Thus, these large IC pulses might have produced TGFs occurring after the IB stage and before the late stage of the two IC flashes. This study provides a set of ground-based observations for comparison to ASIM and other TGF databases.

2. Data sources

Data for this study were obtained with the same combination of instrumentation as described in Stolzenburg et al. (2021). The array of electromagnetic instruments is fully detailed in Marshall et al. (2019) and Bandara et al. (2020), and it included seven stations with a flat-plate fast antenna (decay time constant 10 ms, bandwidth 16 Hz - 2.6 MHz) for E-change data, a LogRF sensor (bandwidth 186-192 MHz) for VHF data, and a dE/dt sensor (bandwidth ~0-2.5 MHz) for time derivative electric field data. At each site, data were recorded (and digitized at 10 MS/s) when the fast antenna detected a pulse exceeding a set trigger threshold, with 250 ms pre-trigger and 150 ms post-trigger. Locations of individual pulses can be determined using a time-of-arrival method termed 'Position by Fast Antenna' (Karunarathne et al., 2013) with the E-change data or the integrated dE/dt data (Bandara et al., 2019) from at least five sites with triggered data. In this work we use the integrated dE/ dt ($\int dE/dt$) pulse locations, in part because it is more sensitive for smaller amplitude pulses. Average location errors in (x, y, z) for located pulses in the two flashes herein are (30, 101, 229) meters and (52, 128, 294) meters. Peak currents of large E-change pulses are estimated using their range-normalized E-change amplitude (normalized to 100 km, averaged from stations >20 km from the pulse) and then applying a multiplying factor of 30 kA per V/m which is derived from the model results in Karunarathne et al. (2021) for large and complicated bipolar IC pulses. We calculate VHF source power for larger events using the Friis equation and method described in Bandara et al. (2019).

The optical data were acquired with a Vision Research Phantom $^{\text{TM}}$ v2512 ultrahigh-speed video camera operated at 150,121 frames/s, or 6.66 μ s frame interval and image exposure of 6 μ s. Frame resolution used was 256 \times 352 pixels, and the camera was fitted with a 14-mm focal length lens. For the two flashes examined herein, individual pixel sizes are approximately 51 m and 46 m on a side, respectively. (Range to the flashes and full image sizes are given below in the descriptions.) As in Stolzenburg et al. (2021) we use the cumulative intensity across each image for analysis of these diffuse events. Cumulative intensity is simply the sum of all the pixel intensity values in each image divided by the total number of pixels (90112). Times and intervals given refer to the end time of the relevant frames, and absolute times have been shifted to arrival time at the central site (EE). In some figures, time axes are labeled

in seconds from 00 UT.

The data presented herein were acquired on 22 June 2019 (UT), when a line of moderately intense thunderstorm cells developed south of the camera site and moved gradually eastward. Reflectivity data from the closest National Weather Service radar (Memphis, approximately 115 km from EE site) are used to describe the storm location and precipitation structure. World Wide Lightning Location Network (WWLLN) data were available for these flashes, including source time and location of detected events. WWLLN time uncertainties are $\sim\!10~\mu\text{s}$, and locations are expected to be within several kilometers (Holzworth et al., 2019).

3. Observations

This study focuses on two typical IC flashes that occurred 163 s apart in approximately the same storm-relative location on 22 June 2019. Both flashes occurred during the active, mature stage of one cell in a short line of multicellular convection that had developed rapidly along a nearly stalled outflow boundary. The storm had started producing lightning about 20 min before these flashes. Pulse locations (shown below) for both flashes indicate they initiated between 8.4 and 9.0 km altitude about 25 km southwest of the camera site and then propagated in a series of IB clusters up to about 11.5 km during their first 10 ms. (A typical IB cluster consists of several narrow IBPs and one classic IBP, see Shi et al. (2019).) Lower altitude activity, with located pulses at 6.3-7.1 km altitude, had sufficiently large amplitude to be located (only) in the few milliseconds prior to each of the large-amplitude E-change events that we focus on herein. Entire flash durations were about 295 ms and 268 ms, and both flashes ended with a bright IC stroke in which visible channel briefly extended out of the cloud. These ending strokes are the only other events detected in each extensive flash that have cumulative intensity maxima exceeding 50% above background. As we show in the following sections, pulse locations of both flashes indicate they were entirely within the camera field-of-view and mainly obscured within cloud. The two flashes studied herein are the only IC flashes known to be captured with ultra-high-speed video during the data acquisition period for which there were very large E-change pulses with coincident large optical signals that were not IB pulses. We will refer to these large bright events as "TC" events, where 'TC' stands for Transient Connector (for reasons described next); this "TC" label also can suggest TGF Candidate (e.g., Marshall et al., 2013).

The first flash (herein referred to as Example A) has three bright events of interest starting at 34.3 ms (referred to as TC1), 45.6 ms (TC2), and 67.3 ms (TC3) after the flash Initiating Event (IE). The second flash (Example B) has two bright events of interest, starting at 18.9 ms (TC4) and 49.8 ms (TC5) after the IE. Each of these five events has a very large amplitude E-change pulse that can be characterized as a Large IC pulse according to the discrimination of Villanueva et al. (1994). The pulse locations during each brief, bright, large-amplitude event span a substantial vertical cloud depth of 3.6-4.3 km, thus Transient Connector (TC) is an appropriate label.. Relative to each flash's IE, these events begin 1.9-2.6 km below and 2.1-4.2 km distance away, and they end 0.9-2.1 km above and 2.7-3.8 km distance away within the region of prior flash activity at upper levels. In this character, our events are similar though apparently not identical to the early stage K events of Shao and Krehbiel (1996). Bright events TC1, TC2, and TC4 are coincident with WWLLN-detected events. In the following sections we describe general features of the two flashes and characteristics of the bright events.

3.1. Example A

This IC flash began at 0434:57.450130 UT with a positive Narrow Bipolar Event (NBE, e.g. Stolzenburg et al., 2021) located at 8.9 km altitude and 25.5 km horizontal distance from the camera site. (The x,y location is -16.3,-19.2; this is 26.7 km range from the 'EE' sensor site.) At this distance, the camera field of view is about 13.1 km across and the

top of the frame is about 17.3 km above the horizon. The *E*-change and VHF data from the EE site for the first 80 ms of Example A are shown in Fig. 1, along with pulse locations (determined from $\int dE/dt$ data at five sites) color-coded by time. Pulse locations are overlaid on the low-level radar reflectivity scan (Fig. 1b) and are projected onto two cross-

sections: through the IE along the camera view angle to the flash (Fig. 1d), and perpendicular, hence approximately along the camera image plane at the range to the IE (Fig. 1e). The flash initiated above the precipitation core, at the top of the 30 dBZ echo. Located IB pulses of the flash show it propagated up to $11.3~{\rm km}$ altitude, into reflectivity <10

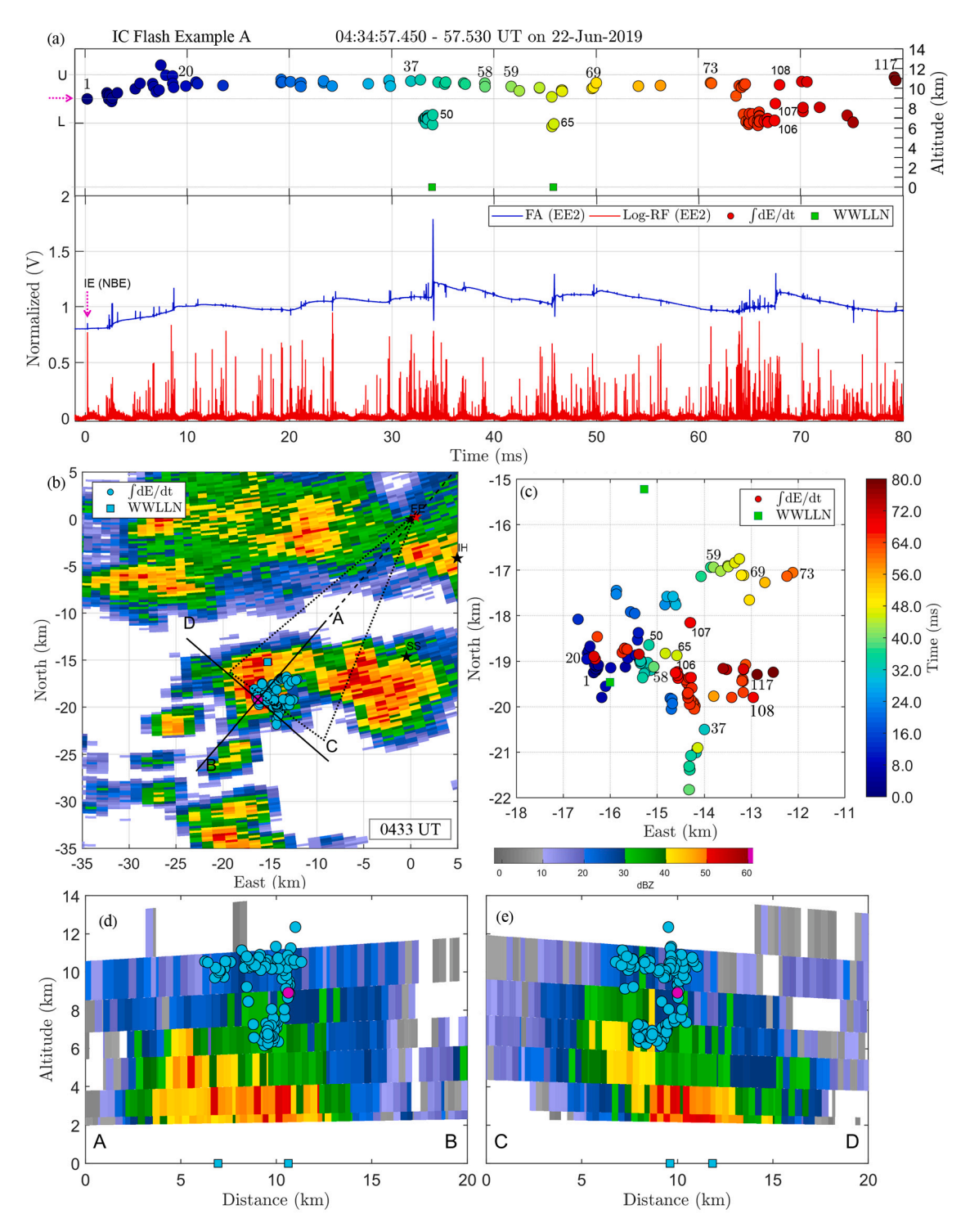


Fig. 1. (a) Time record of *E*-change (FA) and VHF (logRF) data (normalized by largest value) and pulse altitudes (color-coded by time) during first 80 ms of IC flash Example A. Two WWLLN event times translated to EE site are shown at 0 km altitude. (b) Base-scan plan-position indicator of radar reflectivity, with locations of pulses and WWLLN events. First pulse is magenta circle. Locations of camera (red star), approximate camera field of view (dotted triangle), EE and other sensor sites (black labeled stars), and vertical cross-sections through IE are shown. (c) Horizontal (x,y) pulse locations (color-coded by time after 0434:57.450) for first 80 ms of flash. (d) and (e) are vertical cross-sections of reflectivity along camera view (A-B) and approximately along camera image (C—D), with pulse locations projected. Located pulses are identified sequentially for reference; only a few of the numbers are shown in (a) and (c). (For interpretation of the references to color in this figure legend, the reader is referred to the web version of this article.)

dBZ, in the first 10 ms (located pulses numbered 2–19). This upward propagation of negative initial leader occurs in a series of nine IB clusters corresponding to the IB stage (indicated in Fig. 2). The early activity was on the far side of the storm relative to the camera site. Through the next 65 ms, the flash propagated generally toward the camera, with upper level branches centered near 10.5 km altitude extending east, northeast, and southeast, while the less frequently located lower level activity occurred near 6.5 km altitude within 2 km east of the IE (Fig. 1).

The IE (NBE) of this IC flash had VHF power of 71 W and E-change amplitude (range-normalized to 100 km) of 0.43 V/m. Compared to initiator-type positive NBEs in the study by Bandara et al. (2020) in this same region and with similar instrumentation, this NBE is relatively

weak. Six other pulses in the first 72 ms of this flash had larger VHF power than the IE. Fig. 2 includes the cumulative intensity data from the high-speed video recording for the first 72 ms of Example A. At the time of the IE the video camera detected only a very weak increase (< 5% above background) in cumulative intensity within the image. This is similar to weak light enhancements observed with other IC flash IEs, including IEs that are positive NBEs, as described by Stolzenburg et al. (2021). The video data show a larger intensity enhancement during the IB stage, by as much as $\sim\!13\%$ above background value, associated with the first IB cluster. On the basis of several recent studies (e.g., Wilkes et al., 2016; Stolzenburg et al., 2016, 2021) it is likely the IC IB pulses emitted appreciable light, thus we expect that the intensity increases

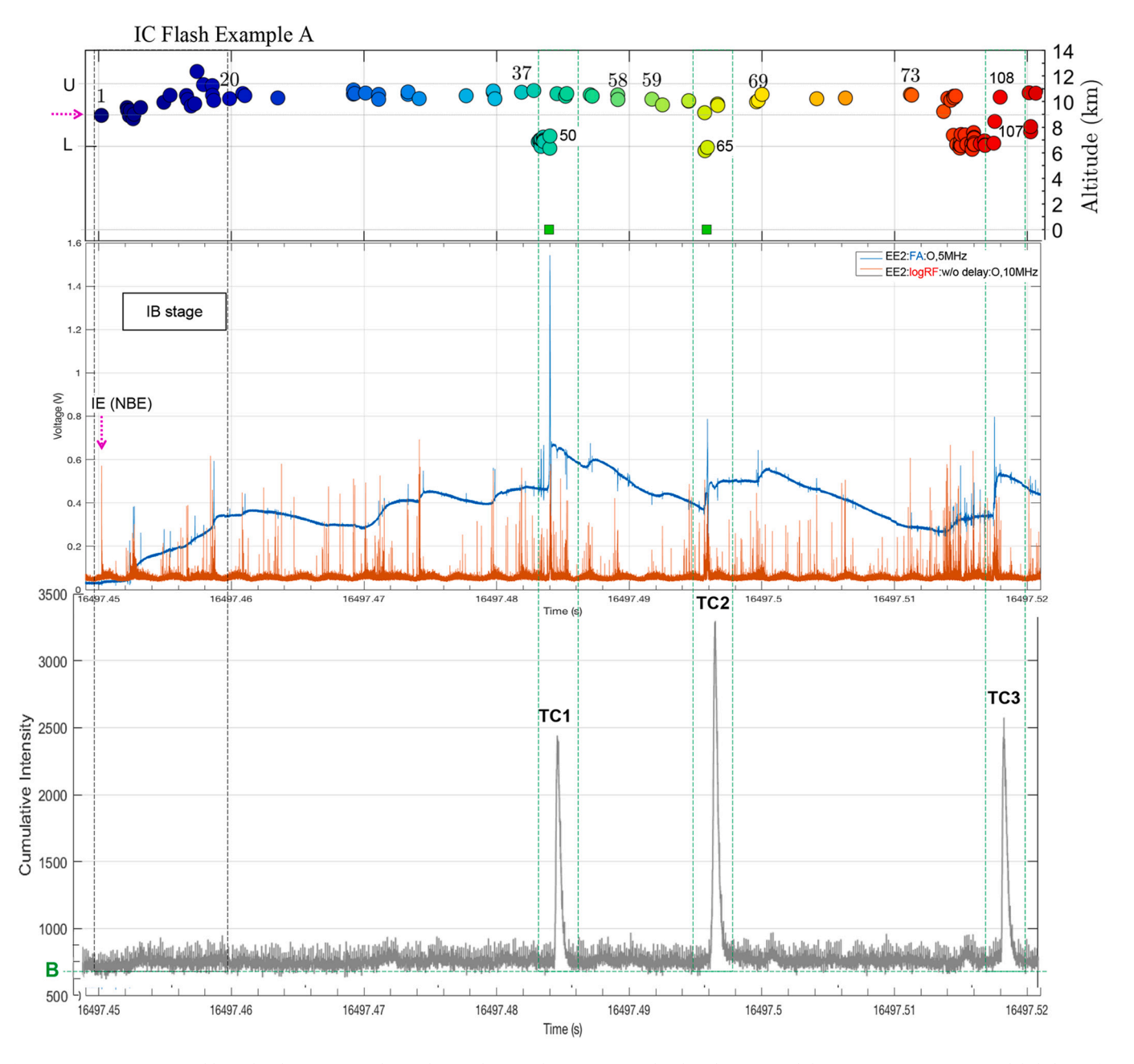


Fig. 2. As in Fig. 1, except calibrated *E*-change (FA) and VHF (logRF) data are shown not normalized, and time period shown (0434:57.450–57.520, labeled in s after 00 UT) is first 72 ms of Example A. Top plot of pulse altitudes (color-coded by time) and two WWLLN event times are from Fig. 1a. Bottom plot is video cumulative intensity for each 6 μs frame exposure in the time period. The initiating event (IE), a positive NBE at 8.9 km altitude, and the IB stage duration are marked. Three 3-ms durations labeled TC1, TC2, and TC3 enclose the large-amplitude, brightly luminous events described in the text and shown in detail in later figures. Horizontal lines in the top plot mark the upper altitude (U, at 11.3 km) of pulse locations reached during the first 10 ms and lower altitude (L, at 6.5 km) of pulse locations reached just before the three large-amplitude events. Line marked B in bottom plot is 10% below background intensity (of 740).

were not well detected by the camera in this case due to the intervening cloud along the viewing angle.

Within 20–60 ms after the IB stage, Fig. 2 shows there were three obvious episodes of bright cumulative intensity, marked TC1, TC2, and TC3, each lasting more than 1 ms. These three bright events are coincident with three of the largest amplitude *E*-change pulses in the flash and with significant VHF activity. The three large amplitude *E*-change pulses resemble the well-known bipolar waveforms of typical IC-type IB pulses (e.g., Marshall et al., 2013), with similar durations and rise times (to peak), but this activity occurs after the IB stage and is obviously larger than anything else in the first 80 ms of this flash. The only other event seen as brightly in the camera data for this entire IC flash occurred

about 225 ms after TC3; it is also described briefly below for comparison.

3.1.1. Event TC1

Data for the time period around TC1 are expanded in Fig. 3. During the 10 ms shown in Fig. 3a and b, there were 22 located pulses (numbers 37–58), and about half these pulses (39–48) were in a small region 1 km east of the IE but lower, at 6.3–7.5 km altitude. This is the first located activity in the flash that is significantly lower than the IE. (The second and third IB clusters each had one pulse located slightly below but within the altitude error bar of the IE.) This low-altitude activity leads on to the main bright TC1 event, which includes pulses 49, 50, and 51.

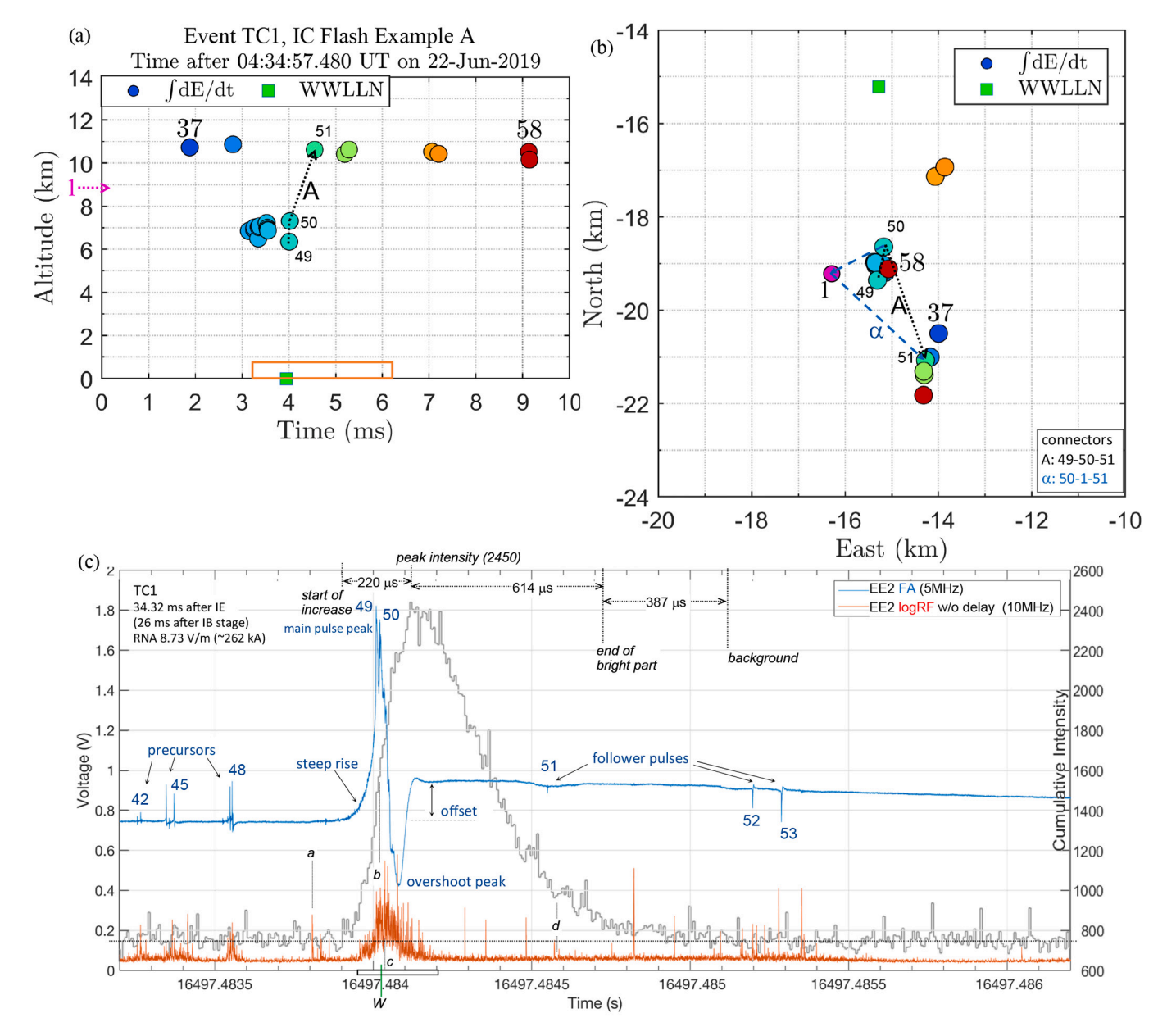


Fig. 3. (a) (b) Time and locations (color-coded) of located pulses during 10 ms surrounding event TC1. Length of segment A (distance between pulses 50 and 51, 520.2 μs apart) is 3.3 km vertical, 2.40 km horizontal; segment labeled α connects pulse 50 to the IE and then to pulse 51. Magenta arrow and circle labeled 1 in (a) and (b) are altitude and location of the flash IE, 30 ms earlier. (c) E-change, VHF, and cumulative intensity data for 3 ms of TC1. Black vertical lines near bottom mark approximate times of the following: a = start of semi-continuous strong VHF and E-change oscillations, b = largest E-change peak (pulse 50; pulse 49, 13.4 μs earlier, has larger peak only at EE site), c = VHF peak in main emission stage, d = end of strong VHF emission. Labeled markers and durations along top relate to the cumulative intensity curve, where 'bright' is considered as >10% above post-event background. Dotted horizontal line indicates average background intensity (~740) before and after enhancement. Full duration of enhanced luminosity is 1.22 ms (183 frames). WWLLN event source time (marked W) is 10.5 μs after source time of pulse 50, with uncertainty (error bar) of +/- 30 μs. (For interpretation of the references to color in this figure legend, the reader is referred to the web version of this article.)

Pulse 49, at 6.35 km altitude, has the largest *E*-change peak at the EE site, although pulse 50 (13.4 μs later, 7.31 km altitude) has the largest range-normalized *E*-change amplitude of 8.73 V/m. (Recall the range-normalized value uses the E-change amplitudes at all sites >20 km from the pulse.) The estimated peak current magnitude, using the relation derived from Karunarathne et al. (2021), is 262 kA. The WWLLN-detected event time during TC1 is 10.5 μs after the largest pulse peak (pulse 50) time and its location is about 4 km north of other activity, hence it is within the expected errors of WWLLN. After translating the respective source locations to the EE site (as shown in Fig. 3) and accounting for uncertainties, the WWLLN event would arrive before the largest *E*-change pulse peak by 20 \pm 30 μs .

The cumulative intensity, E-change, and VHF data for 3 ms including event TC1 are shown in Fig. 3c. Indicators for the start, peak, and end of the bright intensity enhancement (where intensity crosses below 10% above background) are included, along with durations between them. Located pulses in this period are labeled with their numbers, and the WWLLN detection time (translated to EE site) is shown. Markers for the time of the start of steady E-change and VHF oscillations (a), E-change peak (b), strongest VHF emission (c), and approximate end of strong VHF emissions (d) are also shown. The full duration of enhanced luminosity, from the time the increase becomes obvious to when the intensity returns to background, is 1.22 ms, with the brightest portion of this enhancement lasting 834 μ s (or 125 video frames).

The sequence of TC1 (Fig. 3) can be described as follows: after about 20 ms of upper level activity following the IB stage, a series of small but locatable fast pulses (39-48) occurs in a compact region 1-2 km below the IE altitude. About 0.7 ms into this low-altitude activity, the E-change and VHF oscillations both become stronger (time 'a' in Fig. 3c). The detected luminosity begins increasing sharply 90 µs later. The series of small fast pulses lasts about 1 ms and leads up to a very large positive-leading bipolar E-change pulse (number 50) located near but slightly higher altitude than the immediately preceding activity. The steep rise in light intensity and increasing VHF emission continue through the rising side of the large E-change pulse to the E-change peak and WWLLN event. In this case the E-change peak precedes the strongest VHF emission peak of 46 W, while strong VHF occurs for 260 µs throughout the entire bipolar E-change waveform, including another peak (of 62 W) at the time of the overshoot peak in the bipolar pulse. Then, as the E-change pulse returns from its overshoot peak to a positive electrostatic offset value (due to net negative charge moved upward) and the VHF power is decreasing from its maximum, the cumulative light intensity peak is attained. In this case the peak intensity value is 2450, 231% above the background value, and it is reached 220 μs after the beginning of the detectable increase. All parameters decline after the intensity peak, although weaker VHF emissions continue and the gradually decreasing E-change values indicate a continuing current flow. About 0.52 ms after the E-change peak, a relatively small 'follower' pulse (number 51) occurs, located back near the pre-event activity, 3.3 km above and 4.2 km horizontal distance away from the largest Echange pulse. About 10 µs after this follower pulse, the VHF emissions dissipate ('d' in Fig. 3c) and 140 µs later the cumulative intensity decreases to 10% above background. Intensities continue to decline to background level 387 µs later, which we consider the end of this event. Near this ending time the continuing current, indicated by the E-change data offset at EE site, also decreases, just before two additional follower pulses (52 and 53) occur at upper levels and just beyond the first follower pulse location. The time interval of mostly quiet period between follower pulse 51 and pulse 52 is 640 μ s. After pulse 53, weaker continuing current continues but with essentially no VHF activity detected through the next 0.8 ms. Durations, time intervals, and various lengths for data of TC1 shown in Fig. 3 are listed in Table 1, for reference. The duration of the E-change pulse is 222 µs.

As indicated by the segments labeled A in Fig. 3, the altitude difference between pulses 50 and 51 is 3.3 km, and their horizontal separation is also 3.3 km. We cannot be certain, based on the available data,

Table 1Summary characteristics of bright pulse events during two IC flashes.

	TC1	TC2	TC3	TC4	TC5	Average
Pulse IDs: main peak, follower pulse	50, 51	65, 66	107, 108	50, 52	99, 101	
Intensity increase, start to peak (µs)	220	374	233	540	253	324
Intensity, peak to end of bright	614	600	727	660	447	610
(μs) Intensity, bright duration (μs)	834	974	960	1200	700	934
Intensity, end bright to background (µs)	387	527	260	454	553	436
Intensity, enhanced duration (ms)	1.22	1.50	1.22	1.65	1.25	1.37
Intensity peak	2450	3304	2574	2640	1344	2462
value (% above background)	(231)	(346)	(248)	(257)	(82)	(233)
Pulse interval (µs), before to follower	533.6	949.0	484.5		373.0	585.0
main peak to follower	520.2	768.3	403.6	254.5	367.7	462.9
Pulse altitude diff (km), before - follower	4.3	3.7	3.6		4.2	4.0
main peak to follower	3.3	3.4	1.9	4.1	3.8	3.3
Pulse horiz sep (km), before to main	0.7	0.3	1.1		0.7	total horiz avg. 3.0 km
main peak to follower	3.3	2.4	2.1	1.8	2.6	
Est length (km),# before to main peak	1.2	0.4	2.0		0.8	full length avg. 9.6 km
main peak to IE to follower	7.7	9.0	9.3	8.0	9.4	
Time, point a to b* (μs)	215	290	135	550	165	271
Time, point b to c* (μs)	22	-5	-5	50	10	14
Time, point c to d* (μs)	540	990	590	420	580	624
Duration, VHF, point a to d (μs)	775	1275	720	1020	755	909
change pulse	222	199	150	203	134	182
Time, b to peak Intensity* (μs)	+115	+84	+98	-10	+93	+76
Time, b to WWLLN detection*,+ (μs)	10.5	23.4	па	-0.8	па	11 (±12)
E-change amplitude (V/ m) @100 km	8.73	3.81	3.20	8.33	1.62	5.14
Peak current magnitude (kA)	262	114	96	250	49	154
Peak VHF power in main stage (W)	46	21	8	124	36	47
VHF power of nearby peak (W)	62	39	18	154	40	63

[^] End of bright is time when enhanced intensity decreases to 10% above background.

[#] Estimated lengths are (first row) slant distance from 'before' pulse to main pulse, and (second row) from main pulse to 'follower' pulse travelled via the IE

location along horizontal and vertical segments. TC4 has no located 'before' pulse.

 * Points a, b, c, and d refer to the following times (see also Fig. 3): a= start of semi-continuous strong VHF and E-change oscillations, b= largest range-normalized E-change peak, c= VHF peak in main emission stage, d= end of strong VHF emission.

 $^+$ Comparing source times, rather than times received at EE site. Timing errors of WWLLN are $\pm 10~\mu s$.

that these pulse locations are interconnected by channel, especially since the video data show only diffuse light. However, the video data support upward propagation of the increased luminosity through TC1 and through all the five bright events; areas in the middle of the images

get brighter earliest, then the bright intensities move higher in later frames as the event progresses. Hence, if we assume that the pulses during TC1 are directly interconnected by straight paths, then the total altitude spanned in the event, from pulse 49 to 51, is 4.3 km and the cumulative length connecting these three pulses is 5.4 km. Pulses 49 and 51 are 533.6 μ s apart, indicating an average current propagation speed of roughly 1.01×10^7 m/s over the distances between them. Alternatively, we might assume that pulse 50 connects to pulse 51 through the IE location by first traveling along a horizontal path, then upward to the IE, then to the location of pulse 51 along vertical and horizontal paths; this alternative path is indicated by the dashed segments labeled α in Fig. 3. This propagation along previously formed paths back through the

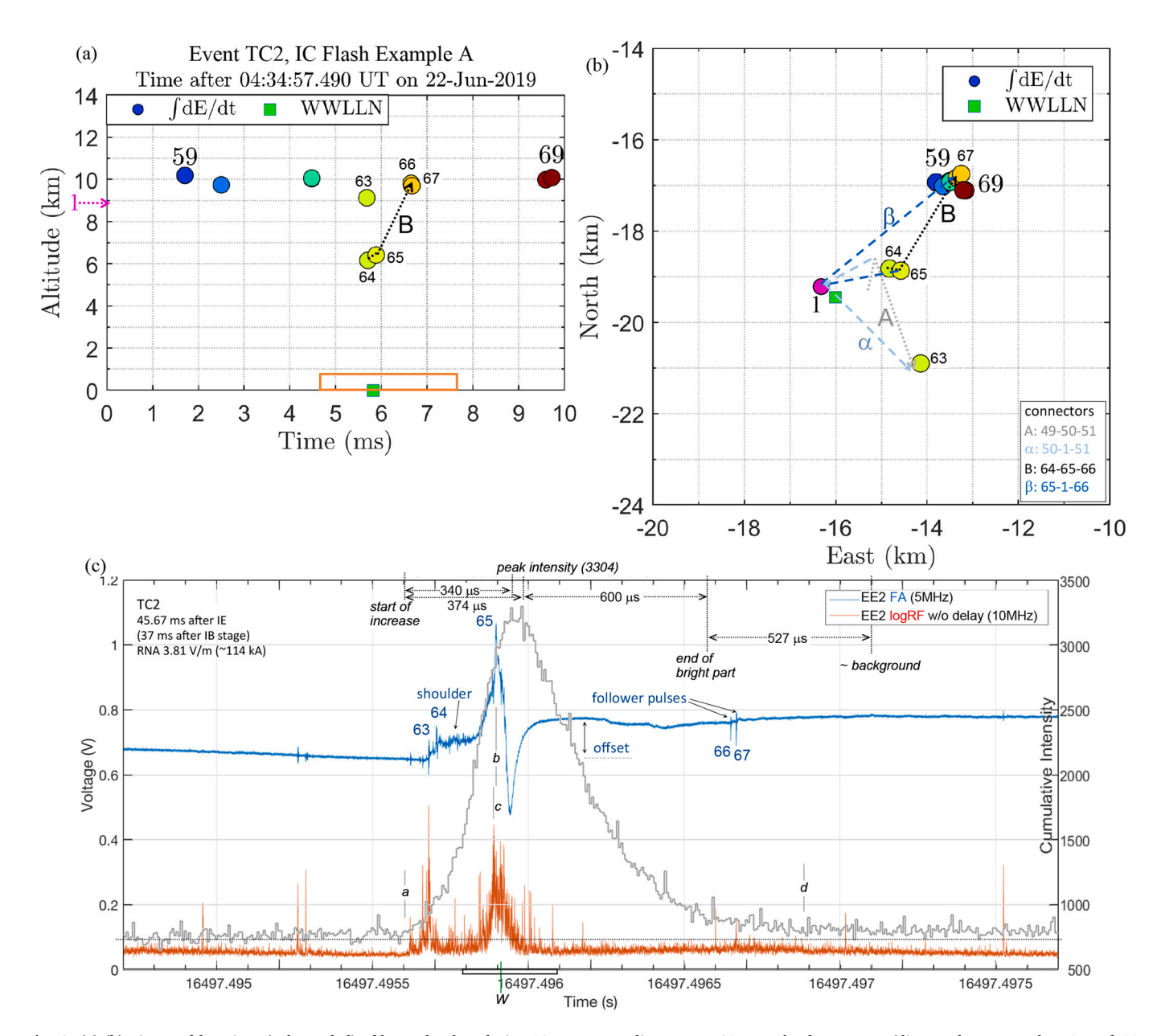


Fig. 4. (a) (b) Time and locations (color-coded) of located pulses during 10 ms surrounding event TC2. Length of segment B (distance between pulses 65 and 66, 768.3 μ s later) is 3.4 km vertical, 2.37 km horizontal; labeled β connects pulse 65 to the IE and then to pulse 66. Magenta arrow and circle labeled 1 in (a) and (b) are altitude and location of the flash IE, 40 ms earlier. Segments A and α (during TC1) x,y locations are overlaid, for reference. (c) E-change, VHF, and cumulative intensity data for 3 ms of TC2. Black vertical lines near bottom mark approximate times of the following: a = start of strong VHF and E-change oscillations, b = largest E-change peak (pulse 65), c = VHF peak in main emission stage, d = end of strong VHF emission. Labeled markers and durations along top relate to the cumulative intensity curve. Dotted horizontal line indicates average background intensity before and after enhancement. Full duration of enhanced luminosity is 1.50 ms (225 frames). WWLLN event source time is 23.4 μ s after source time of pulse 65, with uncertainty (error bar) of $+/-30~\mu$ s. (For interpretation of the references to color in this figure legend, the reader is referred to the web version of this article.)

IE is more reasonable (than direct paths) based on the overall appearance of pulse activity locations for this flash, as shown in Fig. 1d and e. It also fits with the general bi-level horizontal propagation of leader activity after the IB stage in IC flashes and the single mainly vertical path between levels (e.g., Krehbiel et al., 1981; Coleman et al., 2003), and with 'K-event' activity that sometimes travels through the flash initiation region, as mapped with VHF interferometry in Shao and Krehbiel (1996), Akita et al. (2010) and Stock et al. (2014). The alternative cumulative path length, including the 1.2 km between pulses 49 and 50, is 8.9 km, and yields an average current propagation speed of 1.67 \times 10⁷ m/s. For comparison, Karunarathne et al. (2021) modeled several large amplitude IC IBPs and retrieved current speeds that were about a factor of ten faster, $12-18 \times 10^7$ m/s, over lengths of 0.8–1.3 km. Winn et al. (2011) used locations of VHF lightning mapping array data during three K-change events of IC flashes and estimated propagation speeds of $0.33-1.0 \times 10^7$ m/s over lengths of 0.44–1.06 km. Akita et al. (2010) and Stock et al. (2014) found similar ranges of 0.4–1.8 \times 10⁷ m/s for numerous well-mapped K-change events and 'K-leaders' in IC flashes. (In a later section we compare all our estimated speeds to some observed luminosity speeds of leaders and return strokes.)

We note that all the flash activity leading up to TC1 is within the video camera field of view (Fig. 1b). However, there is very little detected luminosity above background level coincident with the upperaltitude activity (located pulses 37–38) nor with the low-altitude precursor activity prior to TC1. These parts of the developing flash are obscured by cloud and/or not very bright. The rapid onset of the very bright luminosity is associated with the increase in VHF emissions and the steep rise in *E*-change values to the main pulse peak, during which the WWLLN event occurs; presumably, this interval would also be when gamma ray emission and a TGF might occur. Light emission continues after the main pulse peak, associated with the subsequent current flow in the presumed upward channel that connects the main pulse and follower pulses. This basic sequence is common to all five large events studied herein.

3.1.2. Event TC2

Expanded views of the data surrounding TC2 are shown in Fig. 4. The 10 ms interval in Fig. 4a and b immediately follows that presented in Fig. 3a and b. In the 5 ms leading up to the TC2 event, the located pulses (numbers 59-62) extend at upper levels (9.7-10.2 km) and eastward from pulses that occurred 8 ms earlier (numbers 55-56, orange in Fig. 3a, b). Beginning at 0434:57.4956 UT (point 'a' in Fig. 4c) there is a series of small, fast pulses in the E-change data, and cumulative intensity starts to increase at the same time as these oscillations begin. The first locatable pulse (63) in this series is at 9.1 km altitude is close to where the pulses a few ms before TC1 and at the end of TC1 occurred (e.g., 37-38, 51). The next locatable pulse (64) is at 6.2 km altitude and close to the location of the low-level activity (pulses 39-48) that preceded TC1. During the series of pulses at the beginning of TC2, the cumulative intensity continues to increase. The E-change data also gradually rise to a quasi-steady larger value for 210 µs prior to the main bipolar pulse; preliminary work by Siedlecki et al. (2017) found this pre-event "shoulder" is a common characteristic in IC pulses associated with WWLLN-detected events in Florida. The WWLLN event time during TC2 is 23 µs after the E-change peak (pulse 65), when the cumulative intensity is still increasing toward its peak. The WWLLN location is about 2 km southwest of pulses 64 and 65, hence within the uncertainties.

At the same time as the E-change oscillations of TC2 begin, Fig. 4c shows the VHF emissions increase and reach an early strong peak (of 39 W) coincident with pulse 63. The VHF emissions slightly subside after pulse 64 but continue at a moderate level through the 210 μ s of the prepulse shoulder in *E*-change data. A second rise in VHF emissions occurs on the rising side of the main bipolar E-change pulse of TC2. In this case the strongest VHF peak (21 W) during the main pulse is 5 μ s before the positive E-change peak, with a secondary similar VHF peak 40 μ s later, during the falling side to the overshoot peak of the E-change pulse.

Strong VHF emissions continue throughout the duration of the main bipolar E-change pulse, 199 $\mu s.$ Weaker, intermittent VHF emission is detected for about 800 μs after the main pulse, as the E-change data return to a positive electrostatic offset value preceding pulse 66. The entire duration of moderate and strong VHF emission in this case (point a to point d) is 1.28 ms. The cumulative intensity decreases to background level about 210 μs later, and total duration of enhanced luminosity is 1.50 ms.

The time of the TC2 event includes located pulses 64, 65, and 66, with a second follower pulse (pulse 67) 18 µs after pulse 66 in the same location. Pulse 65, at 6.4 km altitude, has largest range-normalized Echange amplitude, 3.81 V/m, and 114 kA estimated peak current magnitude. This peak is only about 44% of the E-change amplitude of TC1. However, the light intensity peak of TC2 is 135% that of TC1, and TC2 has longer duration of luminosity enhancement. The segment labeled B in Fig. 4 graphically links pulses 65 and 66, which differ in altitude by 3.4 km and in horizontal position by 2.4 km. If we assume the pulse activity is connected along a direct path, then the altitude spanned in TC2 (pulse 64 to 66), is 3.7 km and the cumulative straight channel length directly connecting these three pulses is 4.5 km. Pulses 64 and 66 are 949.0 μ s apart, yielding an average current speed of roughly 0.48 \times 10⁷ m/s over the intervening distance. Alternatively, if the connection between pulses 65 and 66 is made along a path going first through the IE (as indicated by segments labeled '\beta' in Fig. 4b), then the cumulative length from pulse 64 to 66 is 9.4 km and average current speed is 0.99 \times $10^7 \, \text{m/s}.$

At the beginning of the TC2 main E-change pulse, pulses 63 and 64 are separated by 30 µs, 3.0 km altitude and 2.2 km horizontal distance. It is not clear to us whether the early pulse 63 with concurrent strong VHF emission represents nearly coincident activity occurring in another part of the flash, close to the altitude of the IE, or if it should be considered part of the TC2 event. Including this first (downward) channel part in our estimations would give average speed of 0.84×10^7 m/s through $979 \mu s$ over the direct paths between sequential pulses 63 to 66. As before, if we assume the possible connection between pulses 63 and 64 is through the IE, hence approximately along segment α from TC1, and also assume that pulses 65 and 66 connect back through the IE along segment β , then the total distance is 16.5 km and the average current speed is 1.68×10^7 m/s. This speed is about the same as we estimated for the alternative path (α segments) in TC1. It is intriguing that the total time between pulses 63 and 66 is nearly the same as the duration of the bright part of the cumulative intensity increase associated with TC2, 974 us. As Fig. 4c shows, the enhanced luminosity becomes evident at the same time as the small E-change oscillations begin, about 80 µs before E-change pulse 63 and its coincident strong VHF peak. Durations, time intervals, and lengths for TC2 are listed in Table 1, for reference. Duration of the TC2 E-change pulse, not including the shoulder, is 199

It is evident in Fig. 4b that pulses 64 and 65 of TC2 are close to the low-altitude pulses 49 and 50 of TC1 and its precursor pulses 39-48; together, these locations represent IC flash activity occurring along a (positive) leader tip that propagated down and eastward from the IE to 6.2-7.5 km altitude. During TC1 and TC2, a very large and rapid current apparently travels from the low end to an upper (negative) end, at pulse 51 and 66, respectively, of the branched upper channel. The video data do not show this activity clearly enough to see the paths, but the luminosity moves sequentially from low to high levels (in animation) through each event. Note that immediately prior to event TC1 and its low-altitude precursors there was also upper-altitude activity (e.g., located pulses 37-38 in Fig. 3a and b) in nearly the same location as pulse 63 at the beginning of TC2. The last follower pulses after each event (i.e., pulses 52-53 and 66-67) are located at the apparent extremes of the upper level activity, suggesting the current has travelled the entire channel length.

3.1.3. Event TC3

A few milliseconds after TC2, Example A goes into a relatively quiet and dark period for 10–12 ms, with only a few *E*-change pulses large enough to locate. The next bright event, TC3, includes pulses 106, 107, and 108, and Fig. 5 shows expanded views of the data surrounding TC3. Pulse locations in the 20 ms period (Fig. 5a, b) indicate the upper-level flash activity had spread more eastward by this time. Beginning at 0434:57.514, about 3 ms before TC3, pulse locations show low-altitude activity extends from near the prior low-altitude pulses that occurred before TC1 and TC2 (pulses 39–48, 64–65). This activity progresses northward and culminates at pulse 106, at 6.7 km altitude, which is associated with a large VHF spike and is near the beginning time of the

steep rise in *E*-change. Cumulative intensity starts increasing 60 μs before pulse 106 and rises to peak value in 233 μs . Both the *E*-change and VHF data begin showing larger oscillations at nearly the same time as the intensity starts to increase. During the intensity rise, both the *E*-change pulse peak (pulse 107) and the main stage of strong, continuous VHF emissions occur (with peak values of 8 W and 18 W). The duration of the E-change pulse is 150 μs . The interval between pulses 106 and 107 is 80.9 μs , and their altitudes and horizontal locations are 1.7 and 1.1 km apart, respectively. Moderate and strong VHF emissions continue for about 590 μs after the main pulse peak, and cumulative intensity gradually declines to <10% above background value through 727 μs . Multiple relatively slow E-change oscillations ride the positive offset,

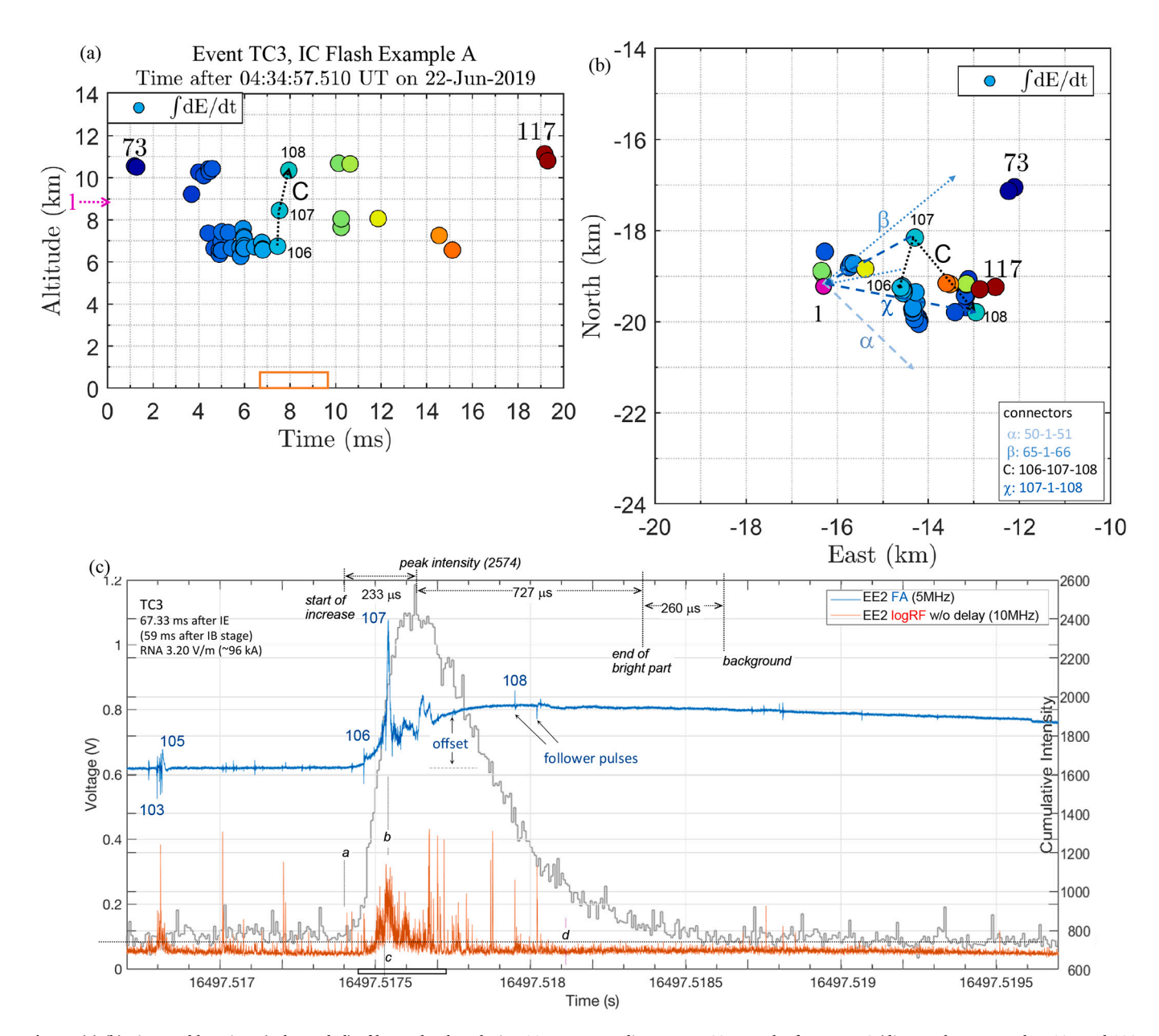


Fig. 5. (a) (b) Time and locations (color-coded) of located pulses during 20 ms surrounding event TC3. Length of segment C (distance between pulses 107 and 108, 403.5 μ s later) is 2.9 km vertical, 2.12 km horizontal; segment labeled χ connects pulse 107 to the IE and then to pulse 108. Magenta arrow and circle labeled 1 in (a) and (b) are altitude and location of the IE, 60 ms earlier. Segments α (during TC1) and β (during TC2) α , volume locations through the IE are overlaid, for reference. (c) E-change, VHF, and cumulative intensity data for 3 ms of TC3. Black vertical lines near bottom mark approximate times of the following: α = start of strong VHF and E-change oscillations, α = largest E-change peak (located pulse 107), α = VHF peak in main emission stage, α = end of strong VHF emission. Labeled markers and durations along top relate to the cumulative intensity curve. Dotted horizontal line indicates average background intensity before and after enhancement. Full duration of enhanced luminosity is 1.22 ms (183 frames). Luminosity of TC3 event is similar to TC1, but no WWLLN detection was recorded with TC3. (For interpretation of the references to color in this figure legend, the reader is referred to the web version of this article.)

masking any apparent overshoot peak in the main E-change waveform of TC3. The only located follower pulse (108) in this event is 403.6 μs after the main E-change peak, although a second pulse (not locate-able) trails pulse 108 by 72 μs .

In most respects, TC3 has characteristics like those of TC1 and TC2. However, the E-change data for TC3 are less similar to the bipolar, IBP-type waveform seen in TC1 and TC2. The main pulse has a mostly positive, nearly unipolar waveform with little overshoot but having a large positive offset similar to TC1 and TC2. TC3 has the fastest rise from

start of oscillations (point a) to the main peak. The main E-change peak amplitude is 3.2 V/m (range normalized) yielding an estimated peak current magnitude of 96 kA, similar to TC2 but only 37% that of TC1. The cumulative intensity curve for TC3 is very similar to that of TC1, with the same overall duration of 1.22 ms and similar peak value and rise time to the peak. As already noted, there is no coincident WWLLN detection with TC3.

As shown in Fig. 5b, locations for the early portion of the upward path in TC3, between pulses 106 and 107, start near the lower portions

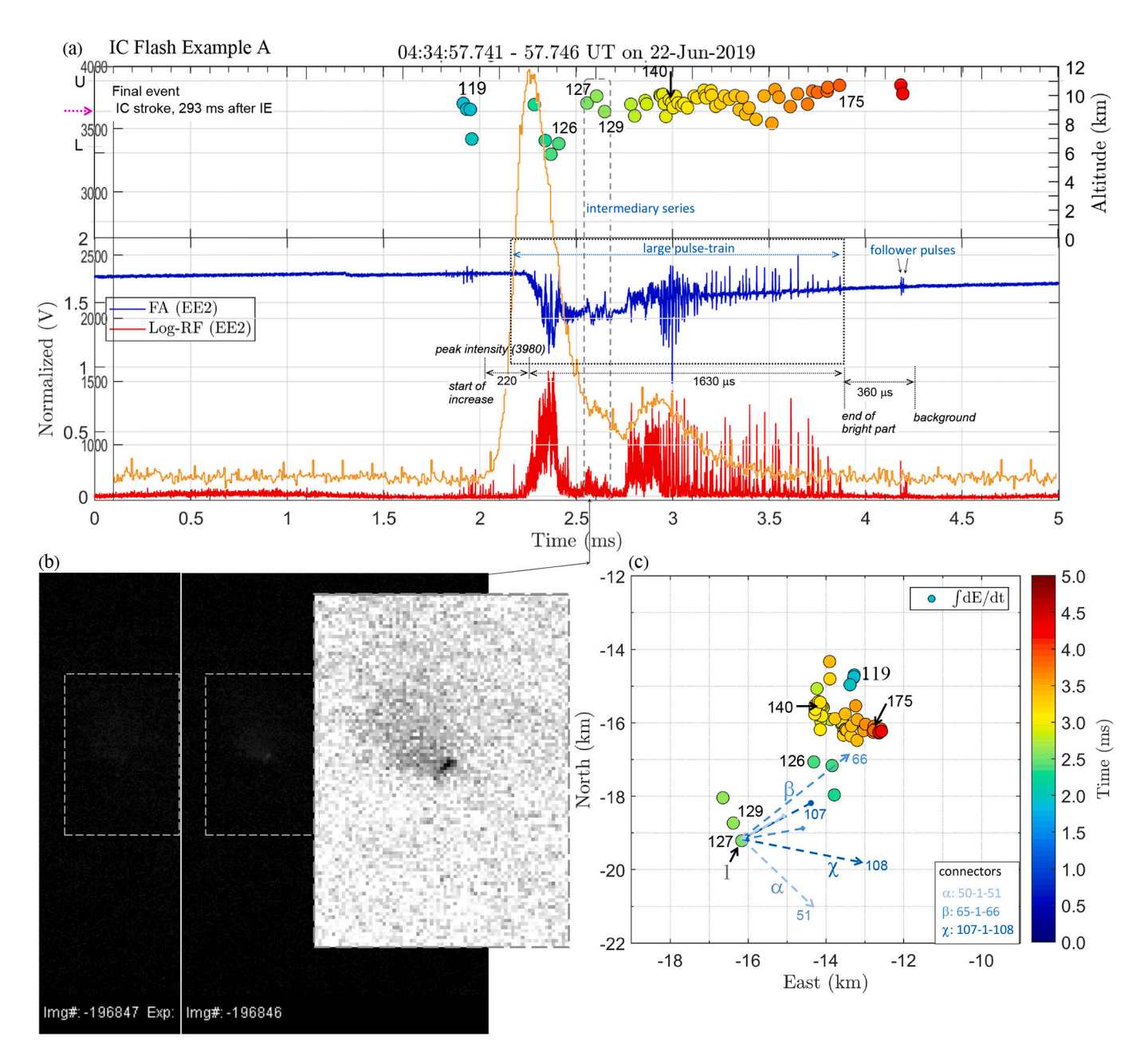


Fig. 6. (a) Time record (5 ms) of E-change (FA) and VHF (logRF) data (normalized by largest value) and pulse altitudes (color-coded by time) during the final event, an IC stroke, of Example A. No WWLLN detection occurred. Cumulative intensity data from video are overlaid (in brown) for the same time period, 0434:57.741–0.746 UT. Indicators and durations of enhanced intensity are included. (b) Center image is full frame, 6 µs exposure, from video camera and (inset right) enlarged, enhanced, inverted gray-scale of outlined portion of same frame, showing channel portion visible during time of pulses 127–128. Image to left is left half (approximately) of prior frame, 6.66 µs earlier. Camera distance to pulse 127 is 25.5 km, at which image pixel size is 51 m per side, top of frame is approximately 17.3 km altitude, brightest pixel is at approximately 9.6 km altitude, and visible channel length is \sim 432–504 m. (c) Horizontal pulse locations (color-coded by time after 0434:57.741) for final 5 ms of located flash activity. Located pulses are identified sequentially in black for reference; only a few of the numbers are shown in (a) and (c). Blue numbers are pulse locations from earlier in the flash, and segments α , β , and γ are the connectors through the IE during TC1, TC2, and TC3. The IE, labeled 1 in Fig. 6c, was 550 m directly below pulse 127 and 293.3 ms earlier. (For interpretation of the references to color in this figure legend, the reader is referred to the web version of this article.)

of TC2 and TC1. The close proximity suggests this early part of TC3 activity may be traveling in the same direction along the path travelled earlier. The later portion (segment χ) of the upward path in TC3, between the IE and follower pulse 108, ends at 10.5 km altitude. Pulse 108 is near the altitude and location of some earlier activity in the 20 ms interval included in Fig. 5a and b. Like the follower pulses of TC1 and TC2, pulse 108 appears at the extremity of the upper level branch activity at the time. The full altitude range of located pulses during TC3 is 3.6 km, similar to TC1 (4.3 km) and TC2 (3.7 km). However, the altitude spanned between the main pulse and the follower pulse in TC3 is much less, due to the higher altitude (8.4 km) of this main pulse. The overall path length in TC3 (from pulse 106 to pulse 108, via pulse 107 and the IE location) is 11.3 km, and the time difference between pulses yields a current speed estimate of 2.33 \times 10 7 m/s, which is faster by 40–135% than estimated for the earlier events.

About 5 ms after TC3 there is a much smaller but similar luminous event (intensities and *E*-change data not shown) between pulses 114 and 117. This relatively weak event, with range-normalized peak E-change amplitude of 1.3 V/m, apparently reconnects the two levels of the flash (6.5 km to 11.1 km) for a fourth time. The cumulative intensity peaks at 1050 (42% above background) and is above background level for 700 us.

3.1.4. Ending event of Example A

The final, and brightest, event in Example A is an extensive IC stroke that occurs about 225 ms after TC3 and about 293 ms after the IE. There was no WWLLN detection during this final event. Activity in this IC stroke begins with moderate VHF emissions and several fast E-change pulses at 9.0–9.4 km altitude at the flash's northeastern extremity (nearest the camera, pulses 119–121), as shown in Fig. 6. In general, the E-change data of the IC stroke (Fig. 6a) are quite different from the E-change data of TC1, TC2, and TC3 (Figs. 3c, 4c, and 5c), so we do not classify this IC stroke as another TC event occurring late in the flash.

Video intensity begins increasing rapidly immediately after these E-change pulses and while the VHF emission continues. Then, starting 365 μ s later (0434:57.7432 UT), the large pulse-train of the stroke begins with a moderately strong VHF event; located pulses indicate this activity is between altitudes of 5.9 km (pulse 125) and 10.8 km (pulse 175). Locations in the pulse train event begin northeast of pulse 107, suggesting the lower level activity earlier in the flash had continued (quietly) extending in that direction after TC3. This region is also approximately below the location of pulses 66–67 (Fig. 4b). After pulse 129, the locations in the large pulse train event extend at upper levels, presumably connecting to the previous activity via the IE location, to the north and east through >5 km horizontally and through 1.2 ms.

Bright luminosity is visible in the camera data (Fig. 6a) for 1.85 ms, with a cumulative intensity peak 4.3 times the background value that is reached 220 µs after the onset. As the brightest part of the IC stroke dims to twice the background level (526 µs after first pulses and start of luminosity rise), there is an intermediary series of five distinct pulses separated by 20-42 µs; the three located pulses in this series (pulses 127-129) are within 140-1220 m horizontal distance and 50-1040 m above the IE. This series is coincident with visible channel or leader extending from the apparent local cloud edge, having estimated length of 432-504 m (diagonally across 6-7 pixels) and seen in the video record for four frames (27 μ s). The first frame of this visible channel and the prior, mostly dark, frame are shown in Fig. 6b. The largest amplitude pulse of the IC stroke (pulse 140, Fig. 6) occurs during the ending period of the E-change pulse train, about 450 µs after the intermediary pulse series; it has estimated peak current of 75 kA and is followed by about 1.2 ms of extensive *E*-change pulse activity centered near 10 km altitude. In the video record, this ending period of the stroke is relatively dim, with peak about twice background, while it is >10% above background until the end of located pulse activity associated with the large pulsetrain event.

Overall, this final event does not have the same appearance in E-change, VHF, or intensity data as the earlier bright TC events in the

flash. However, the final IC stroke is similar to the bright TC1, TC2, and TC3 events in that it also ends with two small 'follower' pulses and these are again located near the apparent extremity of the upper level activity. As shown in Fig. 6, these two pulses occur about 300 µs after the end of the large pulse-train. The IC stroke qualitatively resembles the earlier bright events mainly in its long enhanced luminosity duration and its deep (3-4 km) range of pulse altitudes. Although we lack complete comparative data, it seems likely from the similarity in VHF and Echange data that this IC stroke is the same type of event as fully described by Stock et al. (2017) as a late stage 'K-event' (see, e.g., their Fig. 2), including their 'K-leader' propagation through 340 μs. In particular, the brief positive potential waves, which Stock et al. (2017) term strokes "due to being analogous to the return strokes of negative CG discharges" are apparently fully VHF-mapped versions of the visible channel portion that we see extending outside cloud during pulses 127-129 into a region where no previous activity was observed. The numerous K-events in Stock et al. (2017) Flash 1 all occurred more than 211 ms after IC flash initiation. In our case, this ending event is 293 ms after flash initiation, and the new portion of visible channel extends about 470 m beyond any prior visible activity during one frame interval

3.2. Example B

The second IC flash in this study began at 0437:40.533591 UT with a weak IE located at 8.4 km altitude and 22.9 km distance from the camera. (The x,y position is -10.4, -20.4; range to the EE site is 24.4 km.) The E-change and VHF data for the first 55 ms of Example B are shown in Fig. 7, along with the pulse locations. As for Example A (Fig. 1) pulse locations are overlaid on the low-level radar reflectivity scan (Fig. 7b) and on cross-sections through the IE along the camera view angle (Fig. 7d), and perpendicular, along the camera image plane at the range to the IE (Fig. 7e). Like its predecessor flash, Example B initiated above the precipitation core, in this case beside the highest 30 dBZ echo. (The radar volume nearest in time to Example B is 4 min later than that used for Example A, and the storm moved slightly east-southeastward in the interval.) The located IB pulses show the initial leader propagated mainly upward, to 11.3 km altitude, and into a region with reflectivity of \sim 10–20 dBZ. This upward propagation occurred within the first 10 ms (located pulses numbered 2-28) in several IB clusters comprising the IB stage (indicated in Fig. 8) and was on the far side of the storm relative to the camera.

The weak IE of this IC flash had *E*-change amplitude (range-normalized to 100 km) of 0.073 V/m and no measurable VHF signal. As in Example A, only two of the 25 pulses located with the $\int\!dE/dt$ data during IB stage were below the altitude of the IE, in this case by 300–450 m (hence outside the altitude error bar of the IE location).

Fig. 8 includes the cumulative intensity data from the high-speed video recording for the first 55 ms of Example B. The camera detected only a very weak increase (< 5% above background) in cumulative intensity coincident with the IE, similar to weak light enhancements observed with Example A and other IEs in this dataset (Stolzenburg et al., 2021). The video data during this IB stage also suggest that light emitted with IC IB pulses was mostly obscured from the camera, although there are three intensity enhancements lasting for 600–800 μs coincident with IB clusters and these peak at 10–17% above background.

In the 9–42 ms period after the end of the IB stage, Fig. 8 shows two obvious periods of bright cumulative intensity, marked TC4 and TC5, with durations exceeding 1 ms and peak intensities 82–257% above background value. These bright events are coincident with two of the largest amplitude *E*-change pulses in the flash and with significant VHF activity. There are also two relatively small E-change pulse events between the times of TC4 and TC5 which reach peak cumulative intensities about 35% above background, and both these have substantial VHF activity. Based on available locations, these smaller events apparently

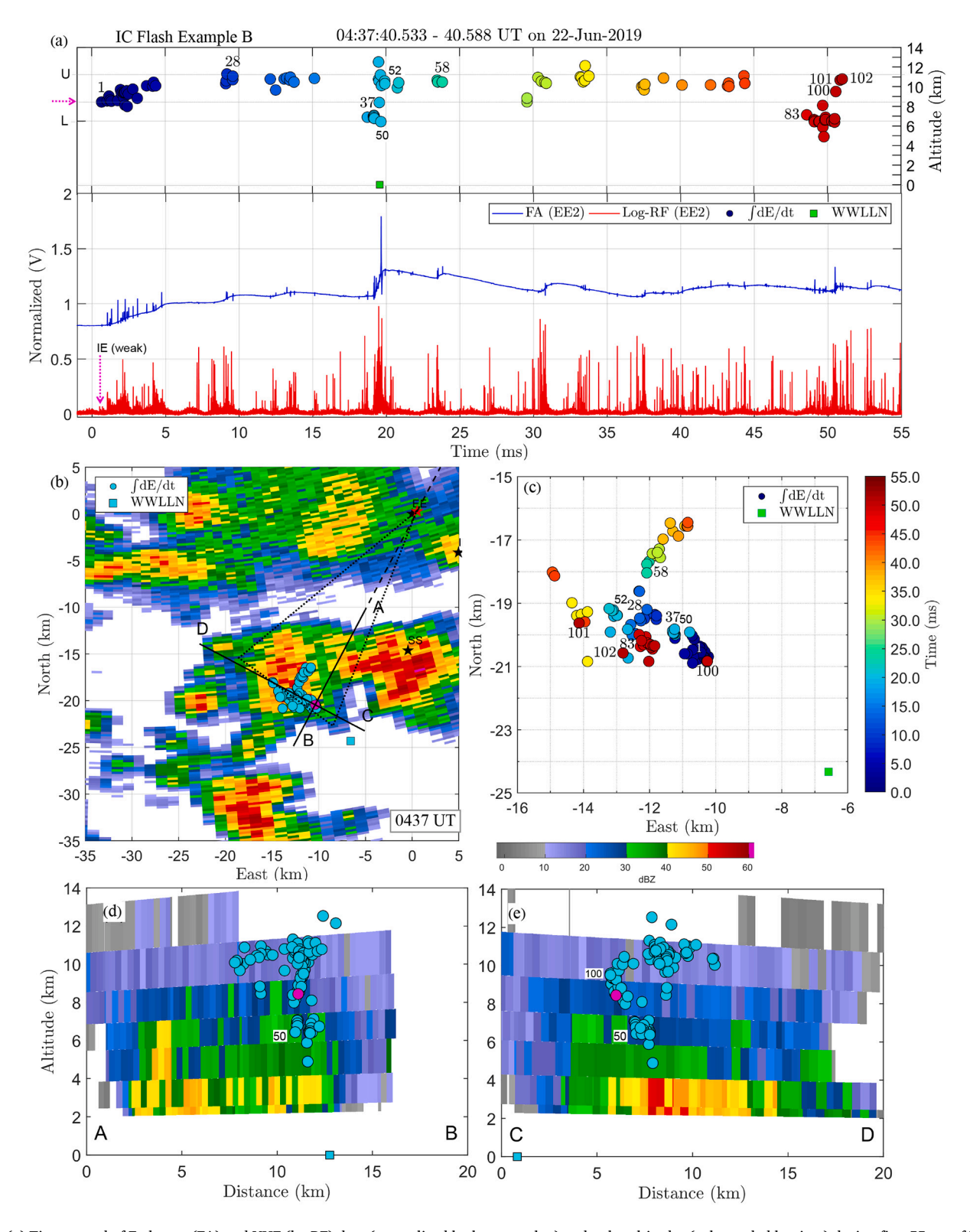


Fig. 7. (a) Time record of E-change (FA) and VHF (logRF) data (normalized by largest value) and pulse altitudes (color-coded by time) during first 55 ms of IC flash Example B. WWLLN event time translated to EE site is shown at 0 km altitude. (b) Base-scan plan-position indicator of radar reflectivity, with locations of pulses and WWLLN event. First pulse is magenta circle. Locations of camera (red star), EE and other sensor sites (black labeled stars), and vertical cross-sections through IE are shown. (c) Horizontal (x,y) pulse locations (color-coded by time after 0437:40.533) for first 55 ms of flash. (d) and (e) are vertical cross-sections of reflectivity along camera view (A-B) and approximately along camera image (C—D), with pulse locations projected. Located pulses are identified sequentially for reference; only a few of the pulse numbers are shown. (For interpretation of the references to color in this figure legend, the reader is referred to the web version of this article.)

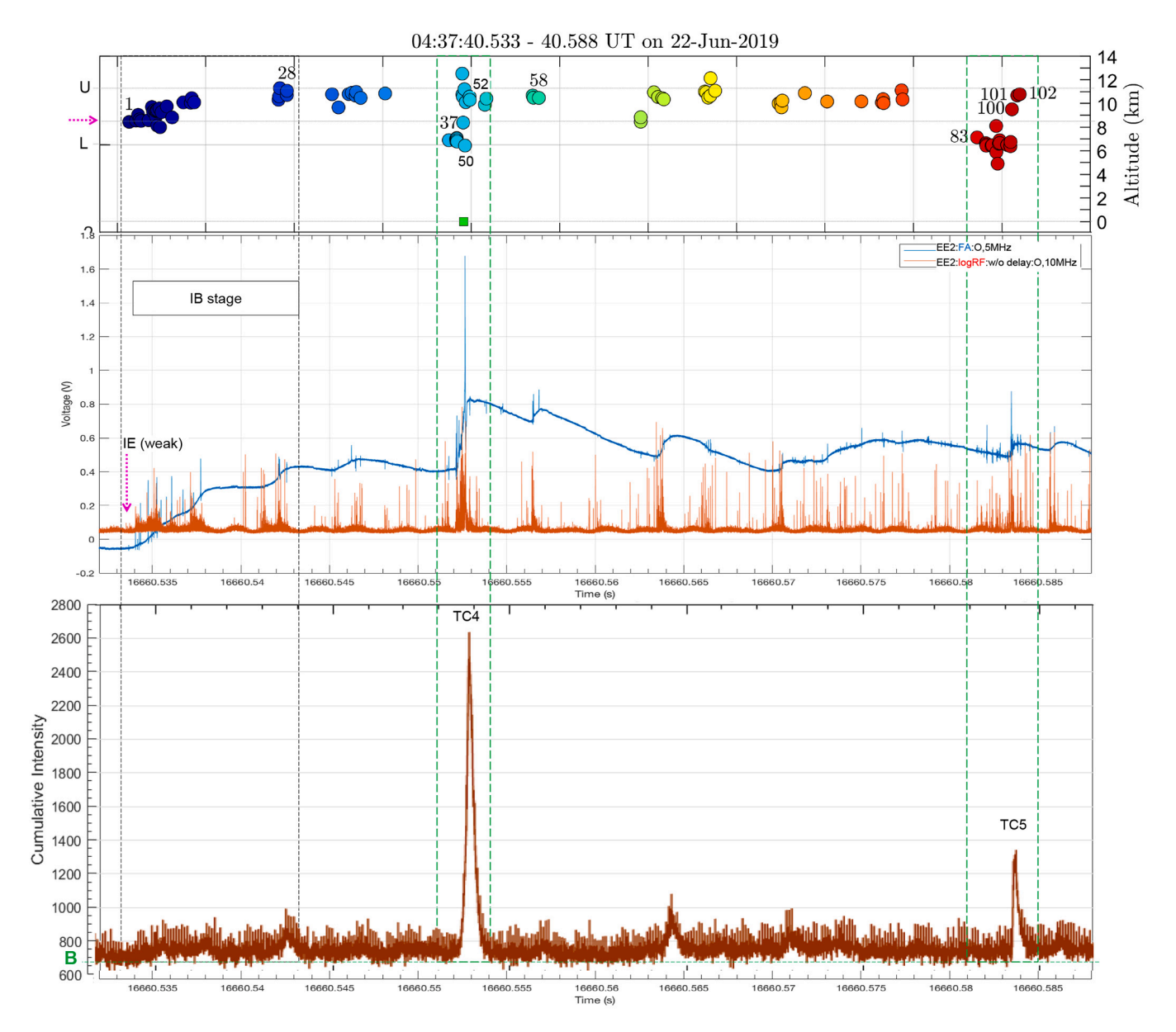


Fig. 8. As in Fig. 7, except calibrated E-change (FA) and VHF (logRF) data are shown not normalized. Time period shown (0437:40.532–40.587, labeled in s after 00 UT) is first 55 ms of IC flash Example B. Top plot of pulse altitudes (color-coded by time) and WWLLN event time are from Fig. 7a. Bottom plot is video cumulative intensity for each 6 μ s frame exposure in the time period. The initiating event (IE), a weak event at 8.5 km altitude, and the IB stage duration are marked. Two durations labeled TC4 (3 ms) and TC5 (4 ms) enclose the large-amplitude, brightly luminous events described in the text and shown in detail in later figures. Horizontal lines in the top plot mark the upper altitude (U, at 11.3 km) of pulse locations reached during the first 10 ms and lower altitude (L, at 6.4 km) of pulse locations reached just before the two large-amplitude events. Line marked B in bottom plot is background intensity (lower envelope of noise).

extend the upper level of the flash; they are much weaker than the events of interest to us herein. The only other event seen brightly in the camera data for this entire IC flash occurred about 214 ms after TC5; it is very similar to the final event in Example A and has peak intensity 167% above background.

3.2.1. Event TC4

Data for the time period around TC4 are shown in Fig. 9. In the 1 ms leading up to the TC4 main pulse, the first low-level activity of this flash that we can locate (pulse 37, Fig. 9a) occurs near 7 km altitude. About 400 µs later, beginning at 0437:40.5521 UT (point 'a' in Fig. 9c) a series of small, fast pulses in the *E*-change data (pulses 38–44) starts, along with continuous VHF emissions, and the cumulative intensity begins increasing at this same time. As with TC2 in Example A (Fig. 4), the main bipolar waveform in TC4 is immediately preceded by an obvious

shoulder of quasi-steady larger values for about 200 μs in the E-change record; this shoulder is associated with some upper level activity (pulses 45–47) and with very strong pulses in the VHF data (peak source power of 320 W), as the cumulative intensity continues to increase. A second rise in VHF emissions occurs during the main bipolar E-change peak, which has duration of 203 μs . In this case the strongest VHF peak (154 W) during the main pulse is at the time of the overshoot peak, with a strong secondary VHF peak (124 W) 50 μs earlier, at the time of the positive E-change peak (pulse 50). Weaker VHF emissions are detected for about 300 μs after the main bipolar E-change pulse ends, during the electrostatic offset. The entire duration of moderate and strong VHF emission (point a to point d) is 1.02 ms. The cumulative intensity decreases to background level about 300 μs after the end of substantial VHF emissions.

Unlike TC1 and TC2, the E-change peak time (pulse 50) in TC4 is

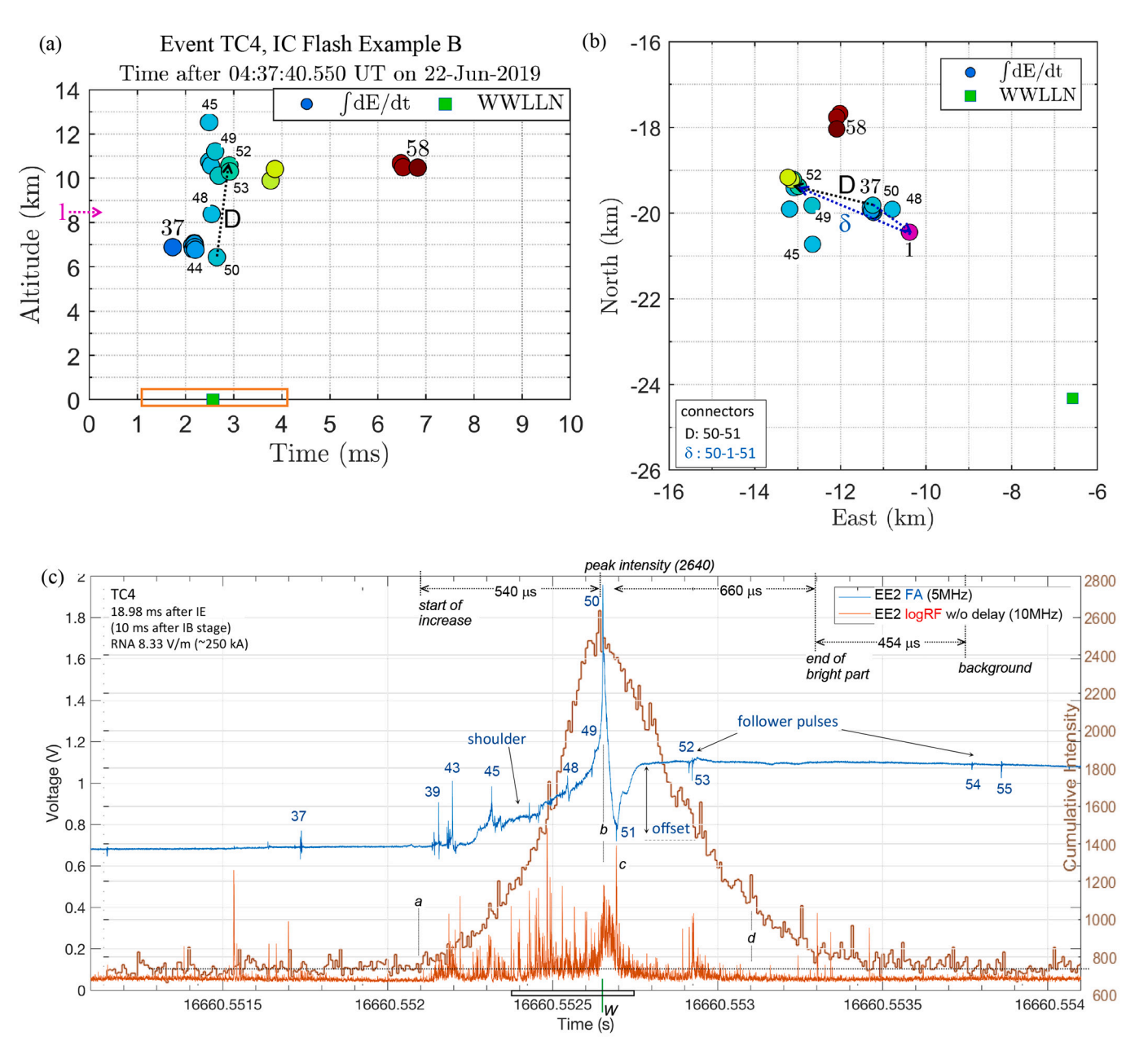


Fig. 9. (a) (b) Time and locations (color-coded) of located pulses during 10 ms surrounding event TC4. Length of segment D (distance between subsequent pulses 50 and 52, 254.5 μ s apart) is 4.1 km vertical, 1.8 km horizontal. Magenta arrow and circle labeled 1 in (a) and (b) are altitude and location of the flash IE, 16.4 ms earlier. Segment labeled δ connects pulses 50 and 52 via the IE. (c) E-change, VHF, and cumulative intensity data for 3 ms of TC4. Black vertical lines near bottom mark approximate times of the following: a = start of strong VHF and E-change oscillations, b = largest E-change peak (pulse 50, largest magnitude peak current), c = VHF peak in main emission stage, d = end of strong VHF emission. Source time of WWLLN is 0.8 μ s before pulse 50. Labeled markers and durations along top relate to the cumulative intensity curve ['bright' is >10% above post-event background]. Dotted horizontal line indicates average background intensity (\sim 740) before and after enhancement. Full duration of enhanced luminosity is 1.65 ms (248 frames). (For interpretation of the references to color in this figure legend, the reader is referred to the web version of this article.)

within 1 μ s of the WWLLN event source time and within 10 μ s of the cumulative intensity peak value. (The WWLLN event location is about 6 km southwest of pulse 50, hence co-located within the system uncertainty.) The light intensity peak of TC4 is 257% above background, similar to TC1 and TC3, but it is reached 540 μ s after the beginning of its increase which is much longer than any of the other events. Overall, the cumulative intensity curve for TC4 appears much more symmetric about the peak because of the slower increase during the *E*-change shoulder. The total duration of luminosity enhancement is 1.65 ms. Durations and other values for TC4 are listed in Table 1, for reference.

The main TC4 event time includes located pulses 48, 50, and 52, while the locations of the intermingled pulses 49 and 51 (Fig. 9) indicate

that activity at upper levels of the flash continues through the event. Pulse 50, at 8.5 km altitude, has *E*-change amplitude of 8.33 V/m, and 250 kA estimated peak current magnitude. Pulse 52 is the first 'follower' pulse, and a subsequent located pulse (pulse 53) is 10 μs later in essentially in the same location. This set of follower pulses is accompanied by a slight increase in cumulative intensity and substantial VHF emission. The segment labeled D in Fig. 9 graphically links pulses 50 and 52, which differ in altitude by 4.1 km and in horizontal position by 1.8 km. As for the other events, if we assume the pulse activity of TC4 is connected along a direct path, then the straight channel length is 4.5 km and average current speed is about 1.78×10^7 m/s. Alternatively, if the connection between pulses 50 and 52 is made along a path going first

through the IE (segments labeled ' δ ' in Fig. 9b), then the cumulative length is 8.0 km and average current speed is 3.15×10^7 m/s. This speed is about twice what we estimated for the alternative paths in TC1 and TC2. Pulse 48 is unlike the 'before' pulses in our other large events because it is higher than the main pulse, with altitude near that of the IE. It is more like the early pulse 63 in TC2, and we are similarly uncertain here whether to consider it a connected part of the main TC4 event or merely concurrent activity in the flash.

As in TC1 and TC2, the large amplitude E-change pulse of TC4 strongly resembles the bipolar waveforms of typical IC-type IB pulses (e. g., Marshall et al., 2013; Karunarathne et al., 2021), with similar duration (203 μ s) and rise time to peak. However, this bright activity

clearly occurs after the IB stage has ended. Like TC1, the TC4 event is larger than most large IB pulses; the largest amplitude found in the study by Smith et al. (2018) was 8.39 V/m, with only three of their largest IB pulses in 40 flashes exceeding 3.0 V/m. These two events are also the largest *E*-change pulses during the entirety of both flashes, by about a factor of two. Like TC2, the E-change data in TC4 has an obvious shoulder, accompanied by strong VHF activity, leading up to the main pulse, and has a large static offset after the pulse. The *E*-change offset (or 'slow' E-change magnitude) in TC4 is 2.8 V/m range-normalized to 100 km, which is very large relative to most K-change (or 'kleine') events.

Soon after TC4 there is a second set of follower pulses: pulses 54 and 55 are 88 µs apart and occur after 840 µs of quiet period after pulse 53.

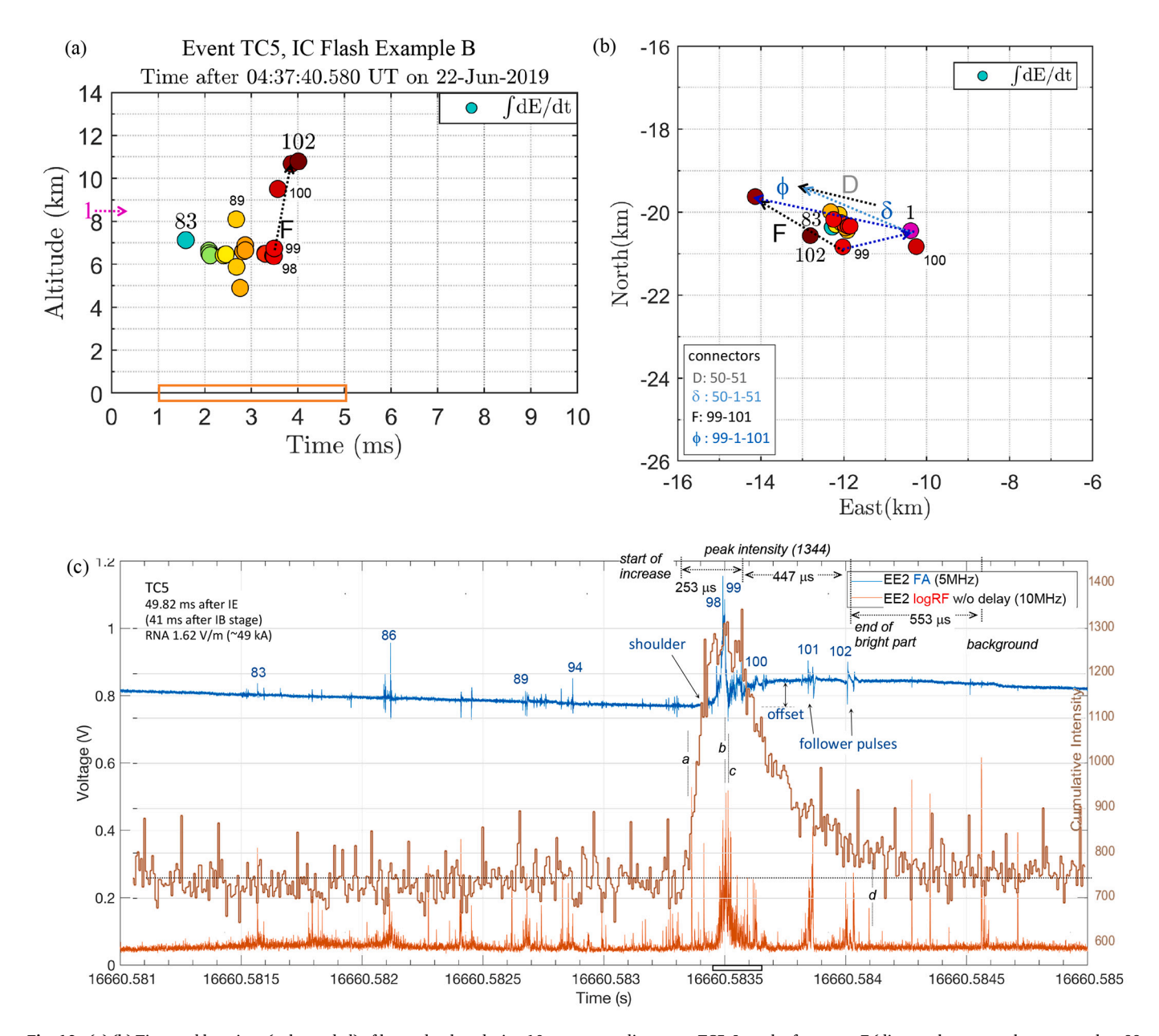


Fig. 10. (a) (b) Time and locations (color-coded) of located pulses during 10 ms surrounding event TC5. Length of segment F (distance between subsequent pulses 99 and 101, 367.7 μ s apart) is 3.8 km vertical, 2.6 km horizontal. Location of segments D and δ , from TC4 (31 ms earlier), also indicated. Magenta arrow and circle labeled 1 in (a) and (b) are altitude and location of the flash IE, 46.4 ms earlier. (c) E-change, VHF, and cumulative intensity data for 4 ms of TC5. Black vertical lines near bottom mark approximate times of the following: a = start of strong VHF and E-change oscillations, b = largest E-change peak (pulse 99; previous peak, pulse 98, is largest only at EE site), c = VHF peak in main emission stage, d = end of strong VHF emission. Labeled markers and durations along top relate to the cumulative intensity curve. Dotted horizontal line is average background intensity (740) before and after enhancement. Full duration of enhanced luminosity is 1.25 ms (188 frames). No WWLLN detection was recorded in this period. (For interpretation of the references to color in this figure legend, the reader is referred to the web version of this article.)

This feature is similar to the TC1 event, with its second set of follower pulses (numbers 52–53 in Example A) occurring 640 μs after its first follower pulse. However, in this case, only the earlier set is accompanied by substantial VHF emission, while in TC1 it was the later set which had some moderately strong VHF. Locations of these four pulses are all at the apparent far end of the branch activity evident (e.g., pulse 49) before TC4, and they are quite close to each other, within 0.3 km horizontally and all in the 9.9–10.6 km altitude range. Throughout this 'follower' period the luminosity continues to steadily decrease, subsiding to 10% above background midway through and to background intensity near the time of pulse 54.

3.2.2. Event TC5

Example B has a relatively dark period lasting about 30 ms after TC4. Upper level branches continue to propagate during this time, but all the pulses we can locate with the multi-station dE/dt data are relatively small and at or above the altitude of the IE. The second large and bright event in this IC flash, TC5, begins about 31 ms after TC4 and includes pulses 98-101. Fig. 10 shows expanded views of the data for the relevant 10 ms

In the 2 ms prior to TC5 (Fig. 10a, b), beginning with pulse 83 at 0437:40.5815 UT, pulse locations indicate lower-level activity (average 6.6 km altitude) about 2 km west of the IE. This activity continues through the time of point 'a' indicated in Fig. 10c, which is approximately when VHF emissions become stronger (with local maximum of 40 W source power) and the small E-change oscillations become more frequent. In this case, the cumulative intensity starts increasing very sharply about 30 µs before point 'a' and rises to a local maximum (in 187 µs) near the time of the largest E-change peak (pulse 99) and the strongest VHF peak (point 'c' is 36 W). A slightly larger cumulative intensity value, the absolute maximum for TC5, occurs 67 µs later. Moderate and strong VHF emissions continue for about 590 μs after the main pulse peak, and cumulative intensity gradually declines to <10% above background value through 447 µs. As seen with TC3, immediately after the positive E-change peak there are multiple E-change oscillations riding the positive offset and masking the overshoot peak. Duration of the main E-change pulse is 134 µs. The only located follower pulse (101) in the first set of these pulses is 367.7 µs after the main E-change peak, then the first in a second set of apparent follower pulses is represented by located pulse 102, 72 µs later.

As shown in Fig. 10b, the location of the main pulse in TC5 is at 6.7 km altitude and is 0.8 km from the apparent end point of the lower-level activity (pulse 98) that precedes it. Like the follower pulses of the other bright events examined herein, pulse 101 appears near the extremity of prior upper level branch activity (e.g., yellow points in Fig. 7c). Pulses 99 and 101 are 3.8 km altitude and 2.6 km distance apart. As in the other bright events, we might assume that the upward path in TC5, between the locations of pulse 99 and 101, connects through the IE. In this case, there is some additional support for such a connection: located pulse 100 occurs in the time between the main and follower pulses and is near the location of the IE. Such an upward path (segment ϕ) in TC5 through the IE to the follower pulse is about 9.5 km long and would indicate a current speed of 2.57×10^7 m/s.

Event TC5 is similar in most ways to TC3 in Example A (Fig. 5), with E-change data having a less bipolar waveform, smaller amplitude, and relatively fast rise from start of oscillations to main peak compared to TC1, TC2 and TC4. The E-change peak amplitude of TC5 is 1.62 V/m and estimated peak current magnitude is 49 kA, which is about half that of TC3 and the smallest of the five events examined herein. The cumulative intensity curve of TC5 is similar in timing and overall duration to those of TC3 and TC1, but with peak value that is also roughly half that of the other bright events. In this case, the intensity curve has a flat peak for nearly 200 μ s, during which the main E-change peak and the main stage of strong VHF emissions occur. There is no coincident WWLLN detection with TC5. The full altitude range of located pulses during TC5 is 4.2 km, similar to TC4 (4.1 km) and TC1 (4.3 km), and the altitude spanned

between the main pulse and the follower pulse is 3.8 km.

Within 2 ms and 13 ms after TC5 there are two much smaller events in Example B; intensities and *E*-change data for the first of these are included near the end of the time period shown in Fig. 8. Similar to the intervening weak events between TC4 and TC5 (e.g., time 16,660.563–0.563 s in Fig. 8) these relatively weak events have no large *E*-change pulses, no activity located below the altitude of the IE, and cumulative intensity peaks of about 900, just 22% above background.

3.2.3. Ending event of Example B

The final event at the end of Example B, like that at the end of Example A, has E-change and VHF data with different character than the earlier bright events in the flashes. We briefly describe and show (in Fig. 11) the data for this IC stroke for comparison, since it qualitatively resembles the earlier bright events in its duration of enhanced luminosity. As for the final event in Example A, it seems likely this event is the same as one type of 'K-event' that is fully described and mapped by Stock et al. (2017).

The final bright event in Example B occurs about 216 ms after TC5 and 263.9 ms after the IE. There were no locations available this late in the flash because only three E-change sites had high time resolution 'triggered' data, but we characterize the event as an IC stroke based on its E-change waveform from the available sensors. Data from the EE site are shown in Fig. 11a. There was no WWLLN detection during this event. Activity in this IC stroke begins with moderate VHF emissions and a short train of relatively small, fast E-change pulses. Video intensity increases rapidly starting about 200 μ s after the VHF emissions begin, and the cumulative intensity peak is reached in 160 μ s. The largest VHF emissions are coincident with the large E-change pulse-train of the stroke, which begins 400 μ s into the event.

Enhanced luminosity occurs in the camera data (Fig. 11a) for 0.79 ms, and the cumulative intensity peak of 1940 (2.6 times background) is reached 220 μs after the onset. As the brightest part of the IC stroke dims to roughly twice the background level (80 µs after the peak luminosity), the large pulse-train associated with the largest E-change pulses and strongest VHF emission occurs. Coincident with the peak in VHF emission and largest E-change amplitude, the video data show a very bright (saturated intensity) channel portion briefly visible extending from the apparent local cloud top. Similar to the final event in Example A, this short, bright channel piece is visible in five frames ($\sim 33~\mu s$). The brightest frame with this visible channel, alongside one image exposed during TC4, are shown in Fig. 11b. As in Example A, our more limited data for this part of the event fit with it being a case of what Stock et al. (2017) term a 'stroke' or brief, positive potential wave that "would propagate back toward and beyond the starting point of the K-leader." In our case, we can say for certain that the visible extent of the channel or leader was at least 92-138 m (2-3 pixels) beyond any earlier visible activity.

About 150 and 200 μs after the largest amplitude pulse of the IC stroke, and after the large pulse-train has ended, there are two large follower pulses that are accompanied by strong VHF peaks; these are the final significant pulses of this flash, 264.6 ms after the IE. The cumulative intensity declines to 10% above background about 100 μs after the second of these two pulses, and then to background level in another 160 μs . All detectable electromagnetic activity of flash Example B ends within 1 ms after this event.

4. Summary

In this study we use ultrahigh-speed video data, with 6 μ s exposure per frame, to investigate two typical IC flashes exhibiting brightly luminous events that occur 19.0–67.3 ms after flash initiation and 10–59 ms after the end of the IB stage. The 'TC' (transient connector) events have bright luminosity, > 10% above background, for 700–1200 μ s duration, and the peak brightness value (i.e., the average pixel intensity within the image) for all but one case is 231–346% above background

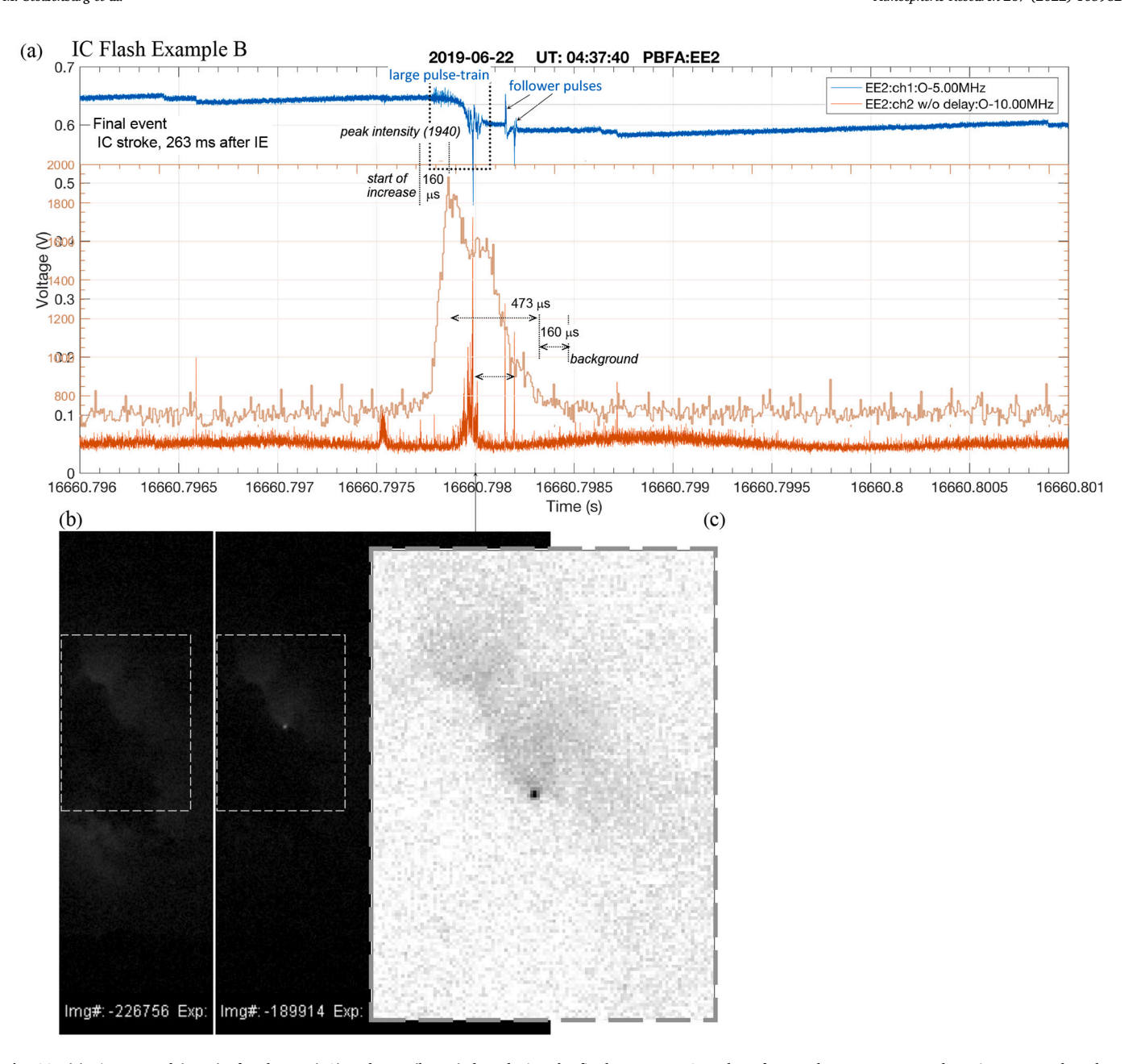


Fig. 11. (a) Time record (5 ms) of E-change (FA) and VHF (logRF) data during the final event, an IC stroke, of Example B. No WWLLN detection occurred, and no pulse locations were available due to insufficient triggered sensor data. Cumulative intensity data from the video record are overlaid (in brown) for the same time period, 0437:40.796–0.801 UT. Indicators and durations of enhanced intensity are included. (b) Center is full frame, 6 μs exposure, from video camera and (inset right) enlarged, enhanced, inverted gray-scale of outlined portion of same frame, showing channel portion visible during event. (Frame ending time is 0437:40.798001 s.) Image shown at left is left half (approximately) of frame exposed 245.415 ms earlier during TC4 event. Camera range to TC4 is 23 km. Image pixel size is 46 m per side at 23 km range, and brightest pixel in the image is at approximately 8.9 km altitude. (For interpretation of the references to color in this figure legend, the reader is referred to the web version of this article.)

intensity. The first IC flash has three of these bright events, two of which have coincident WWLLN detections. The second flash, 163 s later, has two such bright events, and one has a coincident WWLLN detection. During the 295 ms and 268 ms of each extensive IC flash, the camera detected only one other event with maximum cumulative intensity >50% above background level, which was an ending IC stroke or K-event. Corresponding *E*-change data for the bright TC events show that they are associated with large, bipolar (or mainly bipolar) E-change pulses, similar in waveform characteristics to IC-type IB pulses and fitting earlier descriptions of Large IC pulses (e.g., Villanueva et al., 1994). They are qualitatively similar to and perhaps the same as early stage K events described by Shao and Krehbiel (1996). All these bright

TC events have E-change pulse altitudes starting below the flash initiation and ending 3.6–4.2 km higher, i.e., ending near the altitude reached by the initial leader of each flash much earlier, during the IB stage. Corresponding VHF data (186–192 MHz bandwidth) indicate moderate-to-strong emissions start at nearly the same time as the luminosity increase begins, a peak in VHF power (8–124 W) occurs 130–600 μ s later and within 5–50 μ s of the largest E-change pulse, and these VHF emissions last for 720–1275 μ s throughout the duration of bright luminosity. The WWLLN detections occur during strong VHF emissions and within 0–23 μ s of the E-change pulse peak in the three events with largest amplitudes (> 3.8 V/m range normalized to 100 km).

Some characteristics of the cumulative intensity, E-change, and VHF

data for the five bright events (TC1 -TC5) are summarized in Table 1. Luminosity increases rise to peak value in 220-540 µs, with peaks that average 233% above the background cumulative intensity (i.e., 3.33 times background). The main part of the decrease in intensity (down to 10% above background) then occurs less rapidly through 447-727 μs. Full durations of the enhanced luminosity average 1.37 ms. Pulse intervals listed in Table 1 are times between located pulses (from $\int dE/dt$ data) we have identified as the main peak and a 'before' and a 'follower' pulse. (Note that not all small amplitude pulses are locatable, hence the 'before' pulse in each event may not be quite the same; part of the apparent variation among events is due to this variability.) Full intervals of these events range from 373 to 949 μs , and the more clearly identifiable interval from the main peak to follower peak of these bright events averages 463 µs. The time from the beginning evidence of small oscillations in E-change data to the main E-change peak varies from 135 to 550 µs (average 268 µs). The main E-change pulses have durations of 134-222 µs and peak amplitudes averaging 5.14 V/m (normalized to 100 km), yielding average peak current estimate of 154 kA. The strongest VHF powers within the intervals of the events range from 18 to 154

By comparing the detailed figures for each event (Figs. 3, 4, 5, 8, 9) we can summarize the basic character of their waveforms. The overall Echange waveform shapes are similar, large and positive bipolar, having the same polarity as IC IB pulses. The events are immediately preceded by a series of small 'precursor' pulses for about 500 μs . Then, a steep rise (through $\sim\!50\text{--}70~\mu s$) occurs to the main (positive) pulse peak (in TC1, TC3, and TC5) or to the leading 'shoulder' of activity (in TC2 and TC4, with shoulder durations of 150 and 250 μs , before another steep rise to their main peak). After the main peak, the overshoot (negative) peak (having only minor amplitude and short duration in TC3 and TC5) occurs. The E-change values then settle to an electrostatic 'offset' value relative to pre-pulse, which slowly decays (through 5 ms or more, due primarily to the sensor circuit decay-time constant of 10 ms). In each event, at least one and usually two bipolar 'follower' pulses occur within 1 ms after the main pulse indicating each event's end.

As noted, the detected luminosity, main VHF activity, and frequent E-change oscillations of these bright events start at about same time. The precursor activity before the main pulse, which is predominantly at lower altitude, has moderately strong VHF emission, but essentially no luminosity increase is detected this early with these brief pulses. More powerful VHF activity occurs during the steep rise in E-change values (with moderate or strong activity continuing during the 'shoulder' in TC2 and TC4) and during the main bipolar pulse (including the duration of the overshoot pulse in E-change data), all of which overlaps in time with increasing luminosity. A strong VHF peak occurs within 50 μs of main E-change peak, but in each event the strongest VHF is closer in time to the overshoot peak and/or to the first sharp rise in E-change values. The main VHF emission ends when main E-change pulse ends (i. e., settles to its offset value), with some VHF activity during the 'follower' pulses, as the luminosity is dimming to background level.

Despite occurring in two distinct IC flashes, the waveforms of TC2 and TC4 appear *very* similar, except TC4 has larger amplitude and bigger offset. TC4 also has a two-times longer 'shoulder' period of ramp-up before the pulse (with a continued positive *E*-change slope and more strong VHF activity during the shoulder). Likewise, TC3 and TC5 appear *very* similar, except TC5 has smaller amplitude and much smaller offset (both have significant activity for a few ms before, although not all activity before TC3 is shown in Fig. 5); neither of these events has a WWLLN detection.

For comparison and contrast to the bright events accompanying Large IC pulses, we also briefly describe the ending bright event of each flash, both of which we term an IC stroke based on similarity to subsequent strokes in cloud-to-ground flashes. Compared to the range among the five Large IC events studied herein, the ending IC strokes are reasonably similar in peak luminosity and duration: in Flash A, the ending event is brighter and longer, while in Flash B the ending event is

dimmer and shorter than TC1-TC5. However, their E-change waveforms are unlike the Large IC events in overall shape and amplitude. The ending IC strokes are qualitatively similar to each other, including the visible appearance of a short channel piece extending from apparent cloud edge in both. Based on similarities in appearance and flash occurrence timing, these ending events are probably like the late-stage K-events fully described by Stock et al. (2017), including the shorter bursts of 'positive potential waves' during them. Overall, the two flashes studied herein are surprisingly similar and 163 s apart.

In this work we base our interpretation of the IB stage on available locations determined from integrated dE/dt measurements at 5–6 sites, which show the initial leader of both IC flashes reaches the uppermost altitude (approximately 11.5 km) within 10 ms after the IE, during several IB clusters. This interpretation is in keeping with prior work (e. g., Marshall et al., 2013). Unlike previously reported bright events coincident with large bipolar E-change pulses in IC flashes (e.g., Wilkes et al., 2016; Stolzenburg et al., 2021) the events examined in this study all occurred well after the IB stage had ended, and they are not interpreted as IB pulses. In both these flashes, there were no locatable pulses detected below the altitude of the IE until just before the earliest bright event (TC1 and TC4). In each of the five bright events, the located pulses span vertically from \sim 2 km below to \sim 2 km above the IE altitude (at 8.9 km and 8.5 km), and they extend across apparent lengths of 8.9–11.3 km.

For the purpose of estimating and comparing speeds, we tacitly assume the pulse locations are connected by channel along which a current propagates, and further, that this channel probably connects from lowto-high through the IE location. The connection from low-to-high altitude during each bright event is supported by the upward progression of illumination in the video data; the diffuse luminosity increases occur first at mid-frame and then appear higher through subsequent frames in the event. Such paths through the IE location are also in keeping with the overall appearance of pulse locations for the first 80 ms of these two flashes, although we are not able to fully map all the channel locations, and we do not know these bright events actually connect low-to-high (and we do not expect they connect along piece-wise, straight paths). Most importantly, these assumed paths fit with the general, 'I-shaped' appearance of typical IC flashes (e.g., Krehbiel, 1981; Coleman et al., 2003; Stock et al., 2014), with bilevel horizontal activity (negative leaders in upper positive charge and positive leaders in lower negative charge) connected by a single vertical path which includes the flash initiation. Despite the uncertainties herein, the piece-wise length estimates give useful minimum speed estimates. The resulting propagation speeds during the bright events are in the range of $0.99-3.15 \times 10^7$ m/s. As already noted, these apparent speeds are much slower than current speeds determined (via transmission line modeling, $12-18 \times 10^7$ m/s) for large, complicated IB pulses in IC flashes (Karunarathne et al., 2021). The range of estimates is similar to those for K-change events mapped with VHF time-of-arrival and interferometry techniques. For example, Winn et al. (2011) estimated (via sequential VHF source locations) a range of 0.33–1.0 \times 10⁷ m/s for three K-change events of an IC flash. Stock et al. (2014) found, for 27 late-stage, long duration (VHF duration >200 µs) K-events in one flash, 'K-leader' average velocities of 0.4-1.8 \times 10⁷ m/s through lengths of 1.56–16.71 km, and this same range of velocities was found by Akita et al. (2010) for three late-stage K-change events mapped with similar VHF interferometry technique. The current speeds estimated for the bright events herein are also similar to speeds of luminosity advance found for other lightning events occurring inside and below cloud in previously ionized channels. For example, typical dart leader luminosity speeds are $0.5-1.5 \times 10^7$ m/s below cloud base (e.g., Schonland et al., 1935; Jordan et al., 1992) and average 2-D speeds are about 1.7×10^7 m/s over longer lengths and within cloud (Stolzenburg et al., 2013b, 2015). Return stroke luminosity speeds of 0.6–2.0 \times 10⁷ m/s have been observed near the top of the channel (Stolzenburg et al., 2014, 2020), although faster luminosity speeds of 2.9–13 \times 10⁷ m/s are typically observed in the lowest few hundred meters (Orville

and Idone, 1982).

As noted above, the large, bright TC events described herein are similar and possibly the same as the early stage K events detailed by Shao and Krehbiel (1996). The most notable differences between our TC events and the early stage K events of Shao and Krehebiel (1996) (especially events D, G, and H of their Flash A) are (1) the much larger and bipolar fast E-change amplitudes (averaging 5.14 V/m rangenormalized) and larger slow E-change amplitudes (0.9-2.8 V/m) herein, neither of which can be considered 'small' (klein), (2) the relatively early timing of our events, after the IB stage but within the first 80 ms, and (3) the lower altitude relative to flash initiation of the starting points ('before' pulses) in each of our events, including the observation herein that the starting points are not progressively lower for later events in the same flash. These differences also apply to the late-stage K events more frequently studied (e.g., Akita et al., 2010; Stock et al., 2014, 2017) and occurring more than 140 ms after flash initiation. The variations may simply represent the differences among IC flashes among the case studies, however. The additional information herein regarding the very large peak current estimates and the coincident WWLLN detections suggest these types of events occurring after the IB stage and before the late stage deserve further investigation with regard to understanding possible TGF occurrences in IC flashes.

5. Conclusions

Except for the character of their Initiating Events, one of which is an NBE and the other of which is a weak IE, the two IC flashes in this study are extremely similar throughout their 265-295 ms. Both occurred in similar cloud conditions, a few minutes apart, during the mature stage of a moderately strong, quasi-isolated, typical nighttime thunderstorm. In both flashes, the bright 'TC' events focused on in this study accompany large amplitude E-change pulses that are mainly bipolar and have waveforms that resemble Initial Breakdown Pulses. The luminosity characteristics of these bright events also are very similar to those of large IC and IC-type IBPs or IBP clusters studied previously (Stolzenburg et al., 2013a, 2016, 2021; Wilkes et al., 2016), with onset-to-peak intensity times of 220-540 µs and bright intensities lasting about 1 ms. However, we do not interpret these pulses as IBPs, since they occur 10-60 ms after the IB stage, that is, well after the initial (negative polarity) leader of the flashes has reached the upper altitude level of horizontal propagation. The TC events, as described herein, have some characteristics of K-changes or 'K-events' studied previously (e.g., Kitagawa and Brook, 1960; Ogawa and Brook, 1964; Shao et al., 1995; Shao and Krehbiel, 1996; Akita et al., 2010; Stock et al., 2014, 2017), usually with E-change data, which show a relatively small, obvious, step-like variation in 'slow' antenna and unipolar slow modulation in 'fast' antenna during the late stage of a lightning flash. However, these events are unlike most previously studied K-changes, since the E-change pulses are not small (i.e., nicht klein) in amplitude, they are bipolar in shape, and they do not occur during the late stage of the flash. In each case, the locations of E-change pulses show relatively low altitude activity (6-7 km), below the level of the IE (8.5-9 km), occurs just before and at the beginning of each bright event, and then activity proceeds rapidly upward through the IE altitude (and presumably through its horizontal location) and to the upper altitude (10.5-11.5 km) of the flashes' activity (presumably in upper positive charge of the cloud). The motion beginning from ~2 km below the IE is another indication that the E-change pulses are not IBPs, since IBPs of IC flashes develop sequentially upward from the IE (e.g., Marshall et al., 2013; Shi et al., 2019). These pulse locations are supported by generally low-to-high propagation of the diffuse luminosity increases in the video data. The repeating nature of each series, with two or three similar events propagating through similar depths and sequentially increasing extents in the two flashes, makes them similar to the K-events fully described for one IC flash in Stock et al. (2014), except our events all occur much earlier in the flashes and all start much lower in altitude relative to the flash

initiation than the earliest K-events (with durations >200 μ s) in Stock et al. (2014). The propagating current waves have similar speeds, of order 1 \times 10⁷ m/s, as the long 'K-processes' and 'K-leaders' mapped with VHF interferometry by Akita et al. (2010) and Stock et al. (2014) and as the luminosity of dart leaders observed by Stolzenburg et al. (2013b, 2015) over long lengths inside and below clouds in cloud-to-ground flashes.

As introduced in Section 1, Lyu et al. (2015, 2016) have described Energetic IC Pulses (EIPs) as the radio signature of Terrestrial Gamma ray Flashes. Based on our estimated peak current values, which are determined from calibrated E-change amplitudes and known pulse locations, our large bright events TC1 (262 kA), TC2 (114 kA), and TC4 (250 kA) are within or near the range of peak currents estimated for known EIPs. These three events also had WWLLN detections within 0–24 μs of their main E-change pulse peak. The other two events, TC3 (96 kA) and TC5 (49 kA), did not have coincident WWLLN detections but are still considered large for IC pulses. The timing of all five of these large events is not within the first few milliseconds of the IC flashes, hence none are like the EIPs studied previously with known flash context. However, based on their characteristics in E-change, VHF, and cumulative intensity data, we suggest that these large IC events are likely candidates for gamma ray emission and should be the focus of future gamma ray observations.

Funding

This work was supported by the US National Science Foundation [grant number AGS-1745931].

Declaration of Competing Interest

The authors have no conflicting interests to declare.

Acknowledgements

We thank Brian Hurley for vital data collection and management help during the field program. We appreciate the generous assistance of all the site hosts including Martha Mills and North Delta School, Crystal and William McKenzie, Jan Murray, Cherry and Scott Watkins, MRRPMDC Orchards, UM Biological Field Station, UM EE Department, and The Inn at Ole Miss staff. We are always grateful to Sumedhe Karunarathne for critical support of our research. We thank the World Wide Lightning Location Network (http://wwlln.net), a collaboration of over 50 universities and institutions, for providing the WWLLN data used in this paper. We extend special thanks to Richard Orville, for guidance with all aspects of designing and proposing this study, and to staff at TAMU for proposal support. Nicholas Anderson at NSF-PDM is also gratefully acknowledged for efficient assistance and creative solutions. This work is part of NSF grant AGS-1745931. All UM-acquired data used herein are freely available from the corresponding author. Radar data are available from the NOAA/NCEI online repository (https://www. ncdc.noaa.gov/nexradinv/).

References

Abarca, S.F., Corbosiero, K.L., Jr, T.J.G., 2010. An evaluation of the Worldwide Lightning Location Network (WWLLN) using the National Lightning Detection Network (NLDN) as ground truth. J. Geophys. Res. 115, D18206. https://doi.org/10.1029/2009JD013411.

Akita, M., Nakamura, Y., Yoshida, S., Morimoto, T., Ushio, T., Kawasaki, Z., Wang, D., 2010. What occurs in K process of cloud flashes? J. Geophys. Res. 115, D07106. https://doi.org/10.1029/2009JD012016.

Bandara, S., Marshall, T., Karunarathne, S., Karunarathne, N., Siedlecki, R., Stolzenburg, M., 2019. Characterizing three types of negative narrow bipolar events in thunderstorms. Atmos. Res. 227, 263–279. https://doi.org/10.1016/j. atmosres.2019.05.013.

Bandara, S., Marshall, T., Karunarathne, S., Stolzenburg, M., 2020. Electric field change and VHF waveforms of positive Narrow Bipolar events in Mississippi thunderstorms. Atmos. Res. 243 https://doi.org/10.1016/j.atmosres.2020.10500.

- Bils, J.R., Thomson, E.M., Uman, M.A., Mackerras, D., 1988. Electric field pulses in close lightning cloud flashes. J. Geophys. Res. 93, 15933–15940. https://doi.org/ 10.1029/JD093iD12n15933.
- Coleman, L.M., Marshall, T.C., Stolzenburg, M., Hamlin, T., Krehbiel, P.R., Rison, W., Thomas, R.J., 2003. Effects of charge and electrostatic potential on lightning propagation. J. Geophys. Res. 108 (D9), 4298. https://doi.org/10.1029/ 2002/JD002718
- Connaughton, V., Briggs, M.S., Xiong, S., Dwyer, J.R., Hutchins, M.L., Grove, J.E., et al., 2013. Radio signals from electron beams in terrestrial gamma ray flashes. J. Geophys. Res. Space Physics 118, 2313–2320. https://doi.org/10.1029/ 2012.JA018288.
- Cummer, S.A., Lyu, F., Briggs, M.S., Fitzpatrick, G., Roberts, O.J., Dwyer, J.R., 2015. Lightning leader altitude progression in terrestrial gamma-ray flashes. Geophys. Res. Lett. 42, 7792–7798. https://doi.org/10.1002/2015GL065228.
- Fishman, G.J., et al., 1994. Discovery of intense gamma-ray flashes of atmospheric origin. Science 264, 1313–1316.
- Fishman, G.J., et al., 2011. Temporal properties of the terrestrial gamma-ray flashes from the Gamma-Ray Burst Monitor on the Fermi Observatory. J. Geophys. Res. 116, A07304. https://doi.org/10.1029/2010.jA016084.
- Holzworth, R.H., McCarthy, M.P., Brundell, J.B., Jacobson, A.R., Rodger, C.J., 2019. Global distribution of superbolts. J. Geophys. Res. Atmos. 124 (17–18), 9996–10005. https://doi.org/10.1029/2019JD030975.
- Hutchins, M.L., Holzworth, R.H., Rodger, C.J., Brundell, J.B., 2012. Far field power of lightning strokes as measured by the World Wide Lightning Location Network. J. Atmos. Ocean. Technol. 29 (8), 1102–1110. https://doi.org/10.1175/JTECH-D-11.00174 1
- Jordan, D.M., Idone, V.P., Rakov, V.A., Uman, M.A., Beasley, W.H., Jurenka, H., 1992. Observed dart leader speed in natural and triggered lightning. Geophys. Res. Atmos. 97 (D9), 9951–9957. https://doi.org/10.1029/92JD00566.
- Karunarathne, S., Marshall, T.C., Stolzenburg, M., Karunarathna, N., Vickers, L.E., Warner, T.A., Orville, R.E., 2013. Locating initial breakdown pulses using electric field change network. J. Geophys. Res. Atmos. 118 (13), 7129–7141. https://doi. org/10.1002/jgrd.50441.
- Karunarathne, N., Marshall, T.C., Karunarathne, S., Stolzenburg, M., 2021. Modeling initial breakdown pulses of intracloud lightning flashes. Atmos. Res. 261, 105734 https://doi.org/10.1016/j.atmosres.2021.105734.
- Kitagawa, N., Brook, M., 1960. A comparison of intracloud and cloud-to-ground lightning discharges. J. Geophys. Res. 65 (4), 1189–1201.
- Krehbiel, P., 1981. An Analysis of the Electric Field Change Produced by Lightning. PhD thesis. University of Manchester Institute of Science and Technology.
- Lu, G., Blakeslee, R.J., Li, J., Smith, D.M., Shao, X.-M., McCaul, E.W., et al., 2010.
 Lightning mapping observation of a terrestrial gamma-ray flash. Geophys. Res. Lett. 37, L11806. https://doi.org/10.1029/2010GL043494.
- Lyu, F., Cummer, S.A., McTague, L., 2015. Insights into high peak current in-cloud lightning events during thunderstorms. Geophys. Res. Lett. 42, 6836–6843. https://doi.org/10.1002/2015GL065047.
- Lyu, F., Cummer, S.A., Briggs, M., Marisaldi, M., Blakeslee, R.J., Bruning, E., et al., 2016. Ground detection of terrestrial gamma ray flashes from distant radio signals. Geophys. Res. Lett. 43, 8728–8734. https://doi.org/10.1002/2016GL070154.
- Marshall, T., Stolzenburg, M., Karunarathne, S., Cummer, S., Lu, G., Betz, H.-D., et al., 2013. Initial breakdown pulses in intracloud lightning flashes and their relation to terrestrial gamma ray flashes. J. Geophys. Res. Atmos. 118, 10,907–10,925. https:// doi.org/10.1002/jgrd.50866.
- Marshall, T., Bandara, S., Karunarathne, N., Karunarathne, S., Kolmasova, I., Siedlecki, R., Stolzenburg, M., 2019. A study of lightning flash initiation prior to the first initial breakdown pulse. Atmos. Res. 217, 10–23. https://doi.org/10.1016/j.atmosres.2018.10.013.
- Neubert, T., Østgaard, N., Reglero, V., Chanrion, O., Heumesser, M., Dimitriadou, K., et al., 2020. A terrestrial gamma-ray flash and ionospheric ultraviolet emissions powered by lightning. Science 367 (6474), 183–186. https://doi.org/10.1126/science.aax3872.
- Ogawa, T., Brook, M., 1964. The mechanism of the intracloud lightning discharge.

 J. Geophys. Res. 69 (24), 5141–5150. https://doi.org/10.1029/JZ069i024p05141.
- Orville, R.E., Idone, V.P., 1982. Lightning leader characteristics in the thunderstorm research international program (TRIP). J. Geophys. Res. 87, 11,177–11,192. https://doi.org/10.1029/JC087iC13p11177.
- Østgaard, N., Neubert, T., Reglero, V., Ullaland, K., Yang, S., Genov, G., et al., 2019. First 10 months of TGF observations by ASIM. J. Geophys. Res. Atmos. 124 (24), 14024–14036. https://doi.org/10.1029/2019JD031214.
- Østgaard, N., Cummer, S.A., Mezentsev, A., Luque, A., Dwyer, J., Neubert, T., et al., 2021. Simultaneous observations of EIP, TGF, Elve, and optical lightning.

- J. Geophys. Res. Atmos. 126, e2020JD033921 https://doi.org/10.1029/2020JD033921.
- Schonland, B.F.J., Malan, D.J., Collens, H., 1935. Progressive lightning—II. Proc. R. Soc. Lond. Ser. A Math. Phys. Sci. 152 (877), 595–625. https://doi.org/10.1098/rspa.1935.0210.
- Shao, X.M., Krehbiel, P.R., 1996. The spatial and temporal development of intracloud lightning. J. Geophys. Res. 101, 26641–26668.
- Shao, X.M., Krehbiel, P.R., Thomas, R.J., Rison, W., 1995. Radio interferometric observations of cloud-to-ground lightning phenomena in Florida. J. Geophys. Res. 100 (D2), 2749–2783. https://doi.org/10.1029/94JD01943.
- Shi, D., Wang, D., Wu, T., Takagi, N., 2019. Temporal and spatial characteristics of preliminary breakdown pulses in intracloud lightning flashes. J. Geophys. Res. Atmos. 124, 12901–12914. https://doi.org/10.1029/2019JD031130.
- Shi, D., Wang, D., Wu, T., Takagi, N., 2020. A comparison on the E-Change pulses occurring in the bi-level polarity-opposite charge regions of the intracloud lightning flashes. J. Geophys. Res. Atmos. 125 https://doi.org/10.1029/2020JD032996.
- Siedlecki, R.D., Marshall, T.C., Stolzenburg, M., Karunarathne, S., 2017. A study of WWLLN events in Florida thunderstorms. In: Abstract, AGU Fall Meeting, 11-15 Dec. 2017, New Orleans, LA. https://agu.confex.com/agu/fm17/meetingapp.cgi/Pap er/224523.
- Smith, E.M., Marshall, T.C., Karunarathne, S., Siedlecki, R., Stolzenburg, M., 2018. Initial breakdown pulse parameters in intracloud and cloud-to-ground lightning flashes. J. Geophys. Res. Atmos. 123, 2129–2140. https://doi.org/10.1002/2017JD027729.
- Stanley, M.A., Shao, X.-M., Smith, D.M., Lopez, L.L., Pongratz, M.B., Harlin, J.D., et al., 2006. A link between terrestrial gamma ray flashes and intracloud lightning discharges. Geophys. Res. Lett. 33, L06803. https://doi.org/10.1029/2005GL025337
- Stock, M., Akita, M., Krehbiel, P., Rison, W., Edens, H., Kawasaki, Z., Stanley, M., 2014. Continuous broadband digital interferometry of lightning using a generalized cross-correlation algorithm. J. Geophys. Res. Atmos. 119, 3134–3165. https://doi.org/10.1002/2013JD020217.
- Stock, M.G., Krehbiel, P.R., Lapierre, J., Wu, T., Stanley, M.A., Edens, H.E., 2017. Fast positive breakdown in lightning. J. Geophys. Res. Atmos. 122, 8135–8152. https://doi.org/10.1002/2016JD025909.
- Stolzenburg, M., Marshall, T.C., Karunarathne, S., Karunarathna, N., Vickers, L.E., Warner, T.A., Orville, R.E., Betz, H.-D., 2013a. Luminosity of initial breakdown in lightning. J. Geophys. Res. Atmos. 118 https://doi.org/10.1002/jgrd.50276.
- Stolzenburg, M., Marshall, T.C., Karunarathne, S., Karunarathna, N., Warner, T.A., Orville, R.E., 2013b. Stepped-to-dart leaders preceding lightning return strokes. J. Geophys. Res. Atmos. 118, 9845–9869. https://doi.org/10.1002/jgrd.50706.
- Stolzenburg, M., Marshall, T.C., Karunarathne, S., Karunarathna, N., Orville, R.E., 2014. Leader observations during the initial breakdown stage of a lightning flash. J. Geophys. Res. Atmos. 119, 12,198–12,221. https://doi.org/10.1002/2014.ID021994
- Stolzenburg, M., Marshall, T.C., Karunarathne, S., Karunarathna, N., Orville, R.E., 2015. An M-component with a concurrent dart leader traveling along different paths during a lightning flash. J. Geophys. Res. Atmos. 120, 10,267–10,284. https://doi. org/10.1002/2015.1.D023417
- Stolzenburg, M., Marshall, T.C., Karunarathne, S., Orville, R.E., 2016. Luminosity with intracloud-type lightning initial breakdown pulses and terrestrial gamma-ray flash candidates. J. Geophys. Res. 121, 10,919–10,936. https://doi.org/10.1002/ 2016.JD025202.
- Stolzenburg, M., Marshall, T.C., Karunarathne, S., 2020. On the transition from initial leader to stepped leader in negative cloud-to-ground lightning. J. Geophys. Res. Atmos. 125, e2019JD031765 https://doi.org/10.1029/2019JD031765.
- Stolzenburg, M., Marshall, T.C., Bandara, S., Hurley, B., Siedlecki, R., 2021. Ultra-high speed video observations of intracloud lightning flash initiation. Meteorol. Atmos. Phys. https://doi.org/10.1007/s00703-021-00803-3.
- Tilles, J.N., Krehbiel, P.R., Stanley, M.A., Rison, W., Liu, N., Lyu, F., et al., 2020. Radio Interferometer observations of an energetic in-cloud pulse reveal large currents generated by relativistic discharges. J. Geophys. Res. Atmos. 125, 1–22. https://doi. org/10.1029/2020JD032603.
- Villanueva, Y., Rakov, V.A., Uman, M.A., Brook, M., 1994. Microsecond-scale electric field pulses in cloud lightning discharges. J. Geophys. Res. 99, 14,353–14,360. https://doi.org/10.1029/94JD01121.
- Wilkes, R.A., Uman, M.A., Pilkey, J.T., Jordan, D.M., 2016. Luminosity in the initial breakdown stage of cloud-to-ground and intracloud lightning. J. Geophys. Res. Atmos. 121, 1236–1247. https://doi.org/10.1002/2015JD024137.
- Winn, W.P., Aulich, G.D., Hunyady, S.J., Eack, K.B., Edens, H.E., Krehbiel, P.R., et al., 2011. Lightning leader stepping, K changes, and other observations near an intracloud flash. J. Geophys. Res. Atmos. 116 (D23) https://doi.org/10.1029/ 2011.ID015998